

OnsagerNet: Learning Stable and Interpretable Dynamics using a Generalized Onsager Principle

Haijun Yu^{1,*}, Xinyuan Tian¹, Weinan E², and Qianxiao Li^{3,4,*}

¹NCMIS & LSEC, Institute of Computational Mathematics and Scientific/Engineering Computing, Academy of Mathematics and Systems Science, Chinese Academy of Sciences, Beijing 100190, China

²Department of Mathematics and the Program in Applied and Computational Mathematics, Princeton University, Princeton, NJ 08544, USA

³Department of Mathematics, National University of Singapore

⁴Institute of High Performance Computing, A*STAR, Singapore

December 5, 2021

Abstract

We propose a systematic method for learning stable and interpretable dynamical models using sampled trajectory data from physical processes based on a generalized Onsager principle. The learned dynamics are autonomous ordinary differential equations parameterized by neural networks that retain clear physical structure information, such as free energy, diffusion, conservative motion and external force. The neural network representations for the hidden dynamics are trained by minimizing the loss between sample data and predictions using multiple steps of Runge-Kutta methods. For high dimensional problems with a low dimensional slow manifold, an autoencoder with metric preserving regularization is introduced to find the low dimensional generalized coordinates on which we learn the generalized Onsager dynamics. Our method exhibits clear advantages in two benchmark problems for learning ordinary differential equations: nonlinear Langevin dynamics and the Lorenz system. We further apply this method to study Rayleigh-Bénard convection and learn Lorenz-like low dimensional autonomous reduced order models that capture both qualitative and quantitative properties of the underlying dynamics.

keywords machine learning, hidden dynamics, Onsager principle, model reduction, stable and interpretable structure

1 Introduction

Discovering mathematical models from observed dynamical data is a scientific endeavor that dates back to the work of Ptolemy, Kepler and Newton. With the recent advancements in machine learning, a gradual shift is observed from methods relying on human insight to data-driven approaches. The latter has been an active area of research with many proposed methodologies, which can be

* Corresponding authors. E-mail: hyu@lsec.cc.ac.cn(HY), qianxiao@nus.edu.sg(QL)

roughly classified into two categories. The first is *unstructured* approaches, where the learned dynamics are not *a priori* constrained to satisfy any physical principles. Instead, minimizing reconstruction error (or model complexity) is the dominant objective. For example, the sparse symbolic regression method try to find minimal analytic models by searching in a big dictionary of candidate analytic representations [Bongard and Lipson, 2007, Schmidt and Lipson, 2009, Brunton et al., 2016]; Numerical discretization embedding methods try to learn the hidden dynamics by embedding the hidden dynamics with some known numerical discretization into neural networks [Long et al., 2018, Raissi et al., 2018, Xie et al., 2019b]; Galerkin-closure methods use neural networks to complement the projection error of traditional Galerkin methods [Wan et al., 2018, Pan and Duraisamy, 2018, Wang et al., 2020, Ma et al., 2019, Xie et al., 2019a, Wang et al., 2020]. While accurate, these methods suffer from a main drawback: the lack of a theoretical proof of temporal stability, which limits their ability to capture qualitative properties of the underlying model on large time intervals. This is significant in that often, the very point of building reduced models is not to reproduce the original dynamics in its entirety, but rather to extract some salient and physically relevant insights. This leads to the second class of *structured* approaches, where one imparts from the outset some physically motivated constraints to the dynamical system to be learned, e.g. gradient systems [Kolter and Manek, 2019], Hamiltonian systems [Zhong et al., 2020b, Jin et al., 2020], etc. These methods have the advantage that the learned models have pre-determined structures and stability is automatically ensured. However, existing works in this direction have the limitation that the structures imposed are often too restrictive and may not be able to handle complex problems beyond benchmark examples.

In this paper, we propose a systematic method that overcomes the aforementioned limitations. The key idea is a neural network parameterization of a reduced dynamical model, which we call *OnsagerNet*, based on a highly general extension of the Onsager principle for dissipative dynamics [Onsager, 1931a,b]. We choose the Onsager principle, which builds on the second law of thermodynamics and microscopic reversibility, as the starting point due to its simplicity, generality and physical motivation. It naturally gives rise to stable structures for dynamical systems in generalized coordinates, and has been used extensively to derive mathematically well-posed models for complex systems in fluid mechanics, material science, biological science, etc. (see e.g. [Qian et al., 2006][Doi, 2011, Yang et al., 2016, Giga et al., 2017, Jiang et al., 2019]). However, there are two challenges in using it to find dynamical models with high-fidelity:

1. How to choose the generalized coordinates;
2. How to determine the large amount of free coefficients in the structured dynamical system. Some in-depth discussions could be found in Beris and Edwards [1994, Chap 1].

One typical example is the modeling of liquid crystal systems [Doi and Edwards, 1986, De Gennes and Prost, 1993]. If the underlying system is near equilibrium, it is possible to determine the coefficients of a reduced-order (macroscopic) model from mathematical analysis or quasi-equilibrium approximations of the underlying microscopic model (see e.g. Kröger and Ilg [2007], Yu et al. [2010], E [2011], Han et al. [2015]). Otherwise, this task becomes significantly harder, yet a lot of interesting phenomena happen in this regime. Therefore, a method to derive high fidelity macroscopic models that operate far from equilibrium without *a priori* scale information is much sought after.

We tackle these two tasks in a data-driven manner. For the first task we learn an approximately isometric embedding to find generalized coordinates. In the linear case this reduces to the principal

component analysis (PCA), and in general we modify the autoencoder [Hinton and Salakhutdinov, 2006, Rifai et al., 2011] with metric preserving regularization designed for trajectory data. For the second task, we avoid the explicit fitting of the prohibitively large number of response coefficients in linearization approaches. Instead, we parameterize nonlinear relationships between generalized coordinates and the physical quantities governing the dynamics (e.g. free energy, dissipation matrices) as neural networks and train them on observed dynamical data with an embedded Runge-Kutta method. The overall approach of OnsagerNet gives rise to stable and interpretable dynamics, yet retaining a degree of generality in the structure to potentially capture complex interactions. Indeed, the network architecture that we used to parameterize the hidden dynamics has a much more general hypothesis space than other existing structured approaches, and can represent many dynamical systems with physically meaningful origins (e.g. systems described by generalized Poisson brackets). At the same time, the stability of the OnsagerNet is ensured by its internal structure motivated by physical considerations, and this does not reduce its approximation capacity when applied to dynamical data arising from natural processes. We demonstrate the last point by applying the method to the well-known Rayleigh-Bénard convection (RBC) problem, based on which Lorenz discovered a minimal 3-mode ordinary differential equation (ODE) system that presents chaos [Lorenz, 1963]. Lorenz uses three dominant modes in linear stability analysis as reduced coordinates and derives the governing equations by a Galerkin projection. As a severely truncated low-dimensional model, the Lorenz model has limited quantitative accuracy when the system is far from the linear stability region. In fact, it is shown by Curry et al. [1984] that one needs to use more than 100 modes in a Fourier-Galerkin method to get quantitative accuracy for the 2-dimensional RBC problem that is far from the linear region. In this paper, we show that OnsagerNet is able to learn low dimensional Lorenz-like autonomous ODE models with much fewer modes, yet having high quantitative fidelity to the underlying RBC problem. This demonstrates the effectiveness of a principled combination of physics and machine learning when dealing with data from scientific applications.

2 From Onsager principle to OnsagerNet

The Onsager principle [Onsager, 1931a,b] is a well-known model for the dynamics of dissipative systems near equilibrium. Given generalized coordinates $h = (h_1, \dots, h_m)$, their dynamical evolution is modelled by

$$M \frac{dh}{dt} = -\nabla V(h) \quad (1)$$

where $V : \mathbb{R}^m \rightarrow \mathbb{R}$ is a potential function, typically with a thermodynamic interpretation such as free energy or the negated entropy. The matrix M models the energy dissipation of the system (or entropy production) and is positive semi-definite in the sense that $h \cdot Mh \geq 0$ for all h , owing to the second law of thermodynamics. An important result due to Onsager, known as the *reciprocal relations*, shows that if the system possesses microscopic time reversibility, then M is symmetric, i.e. $M_{ij} = M_{ji}$.

The dynamics (1) is simple, yet it can model a large variety of systems close to equilibrium in the *linear response* regime (see e.g. [De Groot and Mazur, 1962, Doi, 2011]). However, many dynamical systems in practice are far from equilibrium, possibly sustained by external forces (e.g. the flow induced transition in liquid crystals [Kröger and Ilg, 2007, Yu et al., 2010]), the kinetic equation

with large Knudsen number [Han et al. \[2019\]](#), etc), and in such cases (1) no longer suffices. Thus, it is an important task to generalize or extend (1) to handle these systems.

The extension of known but limited physical principles to more general domains have been a continual exercise in the development of theoretical physics. In fact, (1) itself can be viewed as a generalization of the Rayleigh’s phenomenological principle of least dissipation for hydrodynamics [[Rayleigh, 1878](#)]. While classical non-equilibrium statistical physics has been further developed in many aspects, including the study of transport phenomena via Green-Kubo relations [[Green, 1954](#), [Kubo, 1957](#)] and the relations between fluctuations and entropy production [[Evans and Searles, 2002](#)], an extension of the dynamical model (1) to model general non-equilibrium systems remains elusive. Furthermore, whether a simple yet general extension with solid physical background exists at all is questionable.

This paper takes a rather different approach. Instead of the possibly arduous tasks of developing a general dynamical theory of non-equilibrium systems from first principles, we seek a *data-driven* extension of (1). In other words, given a dynamical process to be modelled, we posit that it satisfies some reasonable extension of the usual Onsager variational principle, and determine its precise form from data. In particular, we define the *generalized Onsager principle*

$$(M(h) + W(h)) \frac{dh}{dt} = -\nabla V(h) + g(h). \quad (2)$$

where the matrix valued functions M (resp. W) maps h to symmetric positive semi-definite (resp. anti-symmetric) matrices. The last term $g : \mathbb{R}^m \rightarrow \mathbb{R}^m$ is a vector field that represents external forces to the otherwise closed system, and may interact with the system in a nonlinear way. The anti-symmetric term W models the conservative part of the system, and together with g they greatly extend the degree of applicability of the classical Onsager’s principle.

Note that the presence of state (h) dependence on all the terms implies that we are not linearizing the system about some equilibrium state, as is usually done in linear response theory. Consequently, the functions W, M, g and V may be complicated functions of h , and we will learn them from data by parameterizing them as suitably designed neural networks. In this way, we preserve the physical intuition of non-equilibrium physics (dissipation term M , conservative term W , potential term V and external fields g), yet exploit the flexibility of function approximation using data and learning.

We will assume $M(h)+W(h)$ is invertible everywhere, and hence $(M(h)+W(h))^{-1}$ could be written as a sum of a symmetric positive semi-definite matrix, denoted by $\tilde{M}(h)$ and a skew-symmetric matrix, denoted by $\tilde{W}(h)$ (see Theorem 5 in Appendix C for a proof), thus we has an equivalent form for equation (2):

$$\frac{dh}{dt} = -(\tilde{M}(h) + \tilde{W}(h))\nabla V(h) + \tilde{g}(h), \quad (3)$$

where $\tilde{g} = (M + W)^{-1}g$. We will now work with (3) as it is more convenient.

We remark that the form of the generalized Onsager dynamics (2) is not an arbitrary extension of (1). In fact, the dissipative-conservative decomposition $(M + W)$ and dependence on h are well motivated from classical dynamics. To arrive at the former, we make the crucial observation that a dynamical system defined by generalized Poisson brackets [[Beris and Edwards, 1994](#)] have precisely this decomposition (See Appendix A). Moreover, such forms also appeared in partial differential equation (PDE) models for complex fluids [[Yang et al., 2016](#), [Zhao et al., 2018](#)]. Note that general

Poisson brackets are required to satisfy the Jacobi identity (see e.g. [Beris and Edwards, 1994, Ottinger, 2005]), but in our approach we do not enforce such a condition.

The dependence of all terms on h follows from a dimensionality reduction argument: the dynamical system for h is obtained by projecting a higher dimensional system which follows (2) but with constant M, W and g . The dependence on state then arises due to the Jacobian of the projection. In appendix B, we give these derivations. In summary, one can view (2) and (3) both as an extension of the classical Onsager principle to handle systems far from equilibrium, or as a reduction of a high dimensional dynamical system defined by generalized Poisson brackets. Both of these dynamics are highly general in their respective domains of application, and serve as solid foundations on which we build our data-driven methodology.

2.1 Dissipative structure and temporal stability of OnsagerNet

From the mathematical point of view, modeling dynamics using (2) or (3) also has clear advantages, in that the learned system is well-behaved as it evolves through time, unlike unstructured approaches such as dynamic mode decomposition (DMD) (see e.g. Schmid [2010], Takeishi et al. [2017]) and direct parameterization by neural networks, which may achieve a short time trajectory-wise accuracy, but cannot assure mid-to-long time stability as the learned system evolves in time. In our case, we can show in the following result that under mild conditions, the dynamics described by (2) or (3) automatically ensures a dissipative structure, and remains stable as the system evolves in time.

Theorem 1 *The solutions to the system (3) satisfy an energy evolution law*

$$\frac{dV(h)}{dt} = -\|\nabla V(h)\|_{\tilde{M}}^2 + \tilde{g}(h) \cdot \nabla V(h). \quad (4)$$

If we assume further that there exist positive constants α, β and non-negative constants c_0, c_1 such that $h \cdot \tilde{M}h \geq \alpha \|h\|^2$ (uniformly positive dissipation), $V(h) \geq \beta \|h\|^2$ (coercive potential) and $\|\tilde{g}(h)\| \leq c_0 + c_1 \|h\|$ (external force has linear growth). Then, $\|h(t)\|, V(h(t)) < \infty$ for all t . In particular, if there is no external force, then $V(h(t))$ is non-increasing in t .

Proof Equation (4) can be obtained by pairing both sides of equation (3) with ∇V . We now prove boundedness. Using Young's inequality, we have for any ε ,

$$\begin{aligned} \tilde{g}(h) \cdot \nabla V(h) &\leq \varepsilon \|\nabla V(h)\|^2 + \frac{1}{4\varepsilon} \|\tilde{g}(h)\|^2 \\ &\leq \varepsilon \|\nabla V(h)\|^2 + \frac{1}{2\varepsilon} (c_0^2 + c_1^2 \|h\|^2) \end{aligned}$$

Putting the above estimate with $\varepsilon = \alpha$ back to (4), to get

$$\begin{aligned} \frac{dV(h)}{dt} &= -\|\nabla V(h)\|_{\tilde{M}}^2 + \alpha \|\nabla V(h)\|^2 + \frac{1}{2\alpha} (c_0^2 + c_1^2 \|h\|^2) \\ &\leq \frac{c_1^2}{2\alpha\beta} V(h) + \frac{c_0^2}{2\alpha} \end{aligned}$$

By Grönwall inequality, we obtain

$$V(h) \leq \begin{cases} e^{\frac{c_1^2}{2\alpha\beta}t} V_0 + (e^{\frac{c_1^2}{2\alpha\beta}t} - 1) \frac{c_0^2\beta}{c_1^2}, & c_1 > 0, \\ V_0 + \frac{c_0^2}{2\alpha}t, & c_1 = 0, \end{cases}$$

where $V_0 = V(h(0))$. Finally, by the assumption $\|h\|^2 \leq \frac{1}{\beta}V$, h is bounded. Note that when $\tilde{g}(h) \equiv 0$, we have $c_0 = c_1 = 0$, so the above inequality is reduced to $V(h) \leq V_0$, which can be obtained directly from (4) without the requirement of $\alpha > 0, \beta > 0$. \square

Theorem 1 shows that the dynamics is physical under the assumed conditions and we will design our neural network parameterization so that these conditions are satisfied.

3 The OnsagerNet architecture and learning algorithm

In this section, we introduce the detailed network architecture for the parameterization of the generalized Onsager dynamics, and discuss the details of the training algorithm.

3.1 Network architecture

We implement the generalized Onsager principle based on equation (3). $\tilde{M}(h), \tilde{W}(h), V(h)$ and $\tilde{g}(h)$ are represented by neural networks with shared hidden layers and are combined according to equation (3). The resulting composite network is named OnsagerNet. Accounting for (anti-)symmetry, the numbers of independent variables in $\tilde{M}(h), \tilde{W}(h), V(h), \tilde{g}(h)$ are $(m+1)m/2, (m-1)m/2, 1$, and m , respectively.

One important fact is that $V(h)$, as an energy function, should be lower bounded. To ensure this automatically, one may define $V(h) = \frac{1}{2}U(h)^2 + C$, where C is some constant that is smaller than or equal to V 's lower bound. Since the constant C does not affect the dynamics, we drop it in numerical implementation. The actual form we take is

$$V(h) = \frac{1}{2} \sum_{i=1}^m \left(U_i(h) + \sum_{j=1}^m \beta_{ij} h_j \right)^2 + \beta \|h\|^2, \quad (5)$$

where $\beta \geq 0$ is a positive hyper-parameter as assumed in Theorem 1 for forced systems. U_i has a similar structure as one component of $\tilde{W}(h)$. We use m terms in the form (5) to ensure that an original quadratic energy after a dimension reduction can be handled easily. The autograd mechanism implemented in PyTorch [Paszke et al., 2019] is used to calculate $\nabla V(h)$.

To ensure the positive semi-definite property of $\tilde{M}(h)$, we let $\tilde{M}(h) = L(h)L(h)^T + \alpha I$, where $L(h)$ is a lower triangular matrix, I is the identity matrix, $\alpha \geq 0$. Note that the degree of freedom of $L(h)$ and $\tilde{W}(h)$ can be combined into one $m \times m$ matrix. A standard multi-layer perception neural network with ResNet [He et al., 2015] structure is used to generate adaptive bases, which takes (h_1, \dots, h_m) as input, and output $\{L(h), \tilde{W}(h), U_i(h), \hat{f}_i(h)\}$ as linear combinations of those bases. The final output of the OnsagerNet is given by

$$\frac{dh_i}{dt} = \sum_{k=1}^m \left(L(h)L(h)^T + \alpha I + \tilde{W}(h) \right)_{i,k} \left(-\partial_{h_k} V(h) \right) + \hat{f}_i(h), \quad i = 1, \dots, m, \quad (6)$$

where $V(h)$ is defined by (5). Note that in an unforced system we have $\alpha = \beta = 0$, since they are only introduced in forced system to ensure a stability of the learned system as required by Theorem 1. The computation procedure of OnsagerNet is described in Architecture 1.

Architecture 1 $\text{OnsagerNet}(\alpha, \beta, l, n_l; h)$

Input: $h \in \mathbb{R}^m$, parameters $\alpha \geq 0, \beta \geq 0$, activation function σ_A , number of hidden layer l and number of nodes in each hidden layer: n_l

Output: $\text{OnsagerNet}(\alpha, \beta, l, n_l; h) \in \mathbb{R}^m$

- 1: Calculate the shared sub-net output using a l -layer neural network $\phi = \text{MLP}(h) \in \mathbb{R}^{n_l}$. Here MLP has $l - 1$ hidden layer and one output layer, each layer has n_l nodes. Activation function σ_A is applied for all hidden layers and output layer. If $l > 1$, ResNet shortcuts are used.
 - 2: Evaluate U_i using a linear layer as $U_i = \sum_j \omega_{ij}^{(1)} \phi_j + b_i^{(1)}$, calculate V according to (5)
 - 3: Use the autograd mechanism of PyTorch to calculate the gradient $\nabla_{h_k} V(h)$, $k = 1, \dots, m$.
 - 4: Evaluate $A \in \mathbb{R}^{m^2}$ as $A_i = \sum_j \omega_{ij}^{(2)} \phi_j + b_i^{(2)}$.
 - 5: Reshape A as a $m \times m$ matrix, take its lower-triangular part including the main diagonal as L , the upper-triangular part without the main diagonal as \hat{W} .
 - 6: **if** the system is forced **then**
 - 7: calculate the external force/control \hat{f}_i using a priori form.
 - 8: For the forced systems in this paper, we use a linear affine transform $\hat{f}_i = \sum_j \omega_{ij}^{(3)} h_j + b_i^{(3)}$.
 - 9: **else**
 - 10: take $\hat{f}_i = 0$.
 - 11: Calculate the output of OnsagerNet using (6)
 - 12: **return** $\text{OnsagerNet}(\alpha, \beta, l, n_l; h)$.
-

3.2 Training objective and algorithm

To learn ODE model represented by OnsagerNet based on sampled ODE trajectory data, we minimize following loss function

$$\mathcal{L}_{ODE} = \frac{1}{|S|} \sum_{(h(t), h(t+\delta t)) \in S} \frac{1}{\delta t^2} \|h(t + \delta t) - \text{RK2}(\text{OnsagerNet}; h(t), \delta t/n_s, n_s)\|^2. \quad (7)$$

Here δt is the time interval of sample data. S is the sample set. RK2 stands for a second order Runge-Kutta method (Heun method). n_s is the number of RK2 steps used to forward the solution of OnsagerNet from snapshots at t to $t + \delta t$. Other Runge-Kutta method can be used. For simplicity, we only present results using Heun method in this paper. This Runge-Kutta embedding method has several advantages over the linear multi-step methods [Raissi et al., 2018][Xie et al., 2019b], e.g. the variable time interval case and long time interval case can be easily handled by Runge-Kutta methods.

With the definition of the loss function and model architecture, we can then use standard stochastic gradient algorithms to train the network. Here we will use the Adam optimizer [Kingma and Ba, 2015, Reddi et al., 2018] to minimize the loss function with a learning rate scheduler that halves the learning rate if the loss is not decreasing in certain numbers of iterations.

Reduced order model via embedding The previous section describes the situation when no dimensionality reduction is sought or required, and an Onsager dynamics is learned directly on the original trajectory coordinates. On the other hand, if the data are generated from a numerical discretization of some PDE or a large ODE system, and we want to learn a small reduced order

model, then a dimensionality reduction procedure is needed. One can either use linear principal component analysis (PCA) or nonlinear embedding, e.g. the versatile autoencoder, to find a set of good latent coordinates from the high dimensional data. When PCA is used, we do PCA and ODE learning separately. When an autoencoder is used, we can train it either separately or together with the OnsagerNet. The end-to-end training loss function is taken as

$$\begin{aligned}
\mathcal{L}_{tot} &= \mathcal{L}_{AE} + \mathcal{L}_{ODE} + \mathcal{L}_{reg} \\
&= \frac{1}{|S|} \sum_{(u(t), u(t+\delta t)) \in S} \left\{ \beta_{ae} \|u(t) - f_{dec} \circ f_{enc} \circ u(t)\|^2 + \beta_{ae} \|u(t+\delta t) - f_{dec} \circ f_{enc} \circ u(t+\delta t)\|^2 \right. \\
&\quad + \frac{1}{\delta t^2} \|f_{enc} \circ u(t+\delta t) - \text{RK2}(\text{OnsagerNet}; f_{enc} \circ u(t), \delta t/n_s, n_s)\|^2 \\
&\quad \left. + \beta_{isom} \left(\|u(t+\delta t) - u(t)\|^2 - \|f_{enc} \circ u(t+\delta t) - f_{enc} \circ u(t)\|^2 - \alpha_{isom} \right)_+ \right\}, \quad (8)
\end{aligned}$$

where f_{enc} , f_{dec} stands for the encoder function and decoder function of the autoencoder, respectively. In the last term, $\|u(t+\delta t) - u(t)\|^2 - \|f_{enc} \circ u(t+\delta t) - f_{enc} \circ u(t)\|^2$ is an estimate of the isometric loss of the encoder function based on trajectory data, α_{isom} is a constant smaller than the average isometric loss of the PCA dimension reduction. $(\cdot)_+$ stands for positive part. β_{isom} is a penalty constant. β_{ae} is a parameter to balance the autoencoder accuracy and ODE fitting accuracy.

4 Applications

In this section, we present various applications of the OnsagerNet approach. We will start with benchmark problems and then proceed to investigate more challenging settings such as the Rayleigh-Bénard convection (RBC).

4.1 Benchmark problem 1: deterministic damped Langevin equation

Here, we use the OnsagerNet to learn a deterministic damped Langevin equation

$$\frac{dx}{dt} = v, \quad \frac{dv}{dt} = -\frac{\gamma}{m} \frac{dx}{dt} - \frac{1}{m} \nabla_x U(x). \quad (9)$$

Here the resistance γ may be a constant or a parameter that depends on v . For the potential $U(x)$, we consider two cases:

- Hookean spring

$$U(x) = \frac{\kappa}{2} x^2. \quad (10)$$

- Pendulum model

$$U(x) = \frac{4\kappa}{\pi^2} \left(1 - \cos \left(\frac{\pi x}{2} \right) \right). \quad (11)$$

Here no dimensionality reduction is performed and the coordinate $h = (x, v)$ entails the full phase space. The goal of this toy example is to quantify the accuracy and stability of the OnsagerNet, as well as to highlight the interpretability of the learned dynamics.

We normalize the parameter γ, κ by m , i.e. we take $m = 1$. To generate data, we simulate the system using a third order strong stability preserving Runge-Kutta method [Shu and Osher, 1988] for a fixed period of time with initial conditions $\{x_0, v_0\}$ sampled from $\Omega_S = [-1, 1]^2$. Then we use OnsagerNet (6) to learn an ODE system by fitting the simulated data.

In particular, we will demonstrate that the energy V learned has physical meaning. Note that the energy function in the generalized Onsager principle need not be unique. For example, for the heat equation $\frac{du}{dt} = \Delta u$, both $\frac{1}{2}\|u\|^2$ and $\frac{1}{2}\|\nabla u\|^2$ can serve as an energy functional governing the dynamics, with diffusion operators (M matrix) being $-\Delta$ and the identity respectively. The linear Hookean model is similar. Let $V(x, v) = \frac{1}{2}\kappa x^2 + \frac{1}{2}v^2$, then

$$\begin{pmatrix} \frac{dx}{dt} \\ \frac{dv}{dt} \end{pmatrix} = \begin{pmatrix} 0 & 1 \\ -\kappa & -\gamma \end{pmatrix} \begin{pmatrix} x \\ v \end{pmatrix} = - \begin{pmatrix} 0 & -1 \\ 1 & \gamma \end{pmatrix} \nabla V(x, v). \quad (12)$$

The eigenvalue of the matrix $A = \begin{pmatrix} 0 & 1 \\ -1 & -\gamma \end{pmatrix}$ is $\lambda_{1,2} = -\frac{\gamma}{2} \pm \frac{1}{2}\sqrt{\gamma^2 - 4}$. When $\gamma \geq 2$, we always obtain real positive eigenvalues, and the system is over-damped. From equation (12), we may define another energy $\tilde{V}(x, v) = \frac{1}{2}x^2 + \frac{1}{2}v^2$ with dissipative matrix and conservative matrix $-\frac{1}{2}(A + A^T), \frac{1}{2}(A - A^T)$ respectively. For this system, $\hat{V}(x, v) := \tilde{V}(F(x, v))$ with any non-singular linear transform F could serve as energy, the corresponding dynamics is

$$\begin{pmatrix} \frac{dx}{dt} \\ \frac{dv}{dt} \end{pmatrix} = A(F^T F)^{-1} \nabla \hat{V}.$$

Hence, we use this transformation to align the learned energy before making comparison with the exact energy function.

Let us now present the numerical results. We test two cases: 1) Hookean model with $k = 4, \gamma = 3$; 2) Pendulum model with $k = 4$ and $\gamma(v) = 3|v|^2$. To generate sample data, we simulate the ODE systems to obtain 100 trajectories with uniform random initial conditions $(x, v) \in [-1, 1]^2$. For each trajectory, 100 pairs of snapshots at $(iT/100, iT/100 + 0.001), i = 0, \dots, 99$ are used as sample data. Here T is the time period of sampled trajectories, we take it to be 5. Snapshots from the first 80 trajectories are taken as the training set, while the remaining snapshots are taken as the test set.

We test three different methods for learning dynamics: OnsagerNet, symplectic dissipative ODE net (SymODEN [Zhong et al., 2020b]), and a simple multi-layer perception ODE network (MLP-ODEN) with ResNet structure. To make the numbers of tunable parameters in three ODE nets comparable, we choose $l = 1$ and $n_l = 12$ for OnsagerNet, $n_l = 17$ for SymODEN, and MLP-ODEN with two hidden layers and each layer has 9 hidden units, such that the total numbers of tunable parameters in OnsagerNet, SymODEN and MLP-ODEN are 120, 137, and 124, correspondingly.

To test the robustness of those networks paired with different activation functions, five C^1 activation functions are tested, including ReQU, ReQUr, softplus, sigmoid and tanh. Here, ReQU, defined as $(x) := x^2$ if $x \geq 0$, otherwise 0, is the rectified quadratic unit studied in [Li et al., 2020]. Since ReQU is not uniformly Lipschitz, we introduce ReQUr as a regularization of ReQU, defined as $\text{ReQUr}(x) := \text{ReQU}(x) - \text{ReQU}(x - 0.5)$.

The networks are trained using a new version of Adam [Reddi et al., 2018] with mini-batches of size 200 and initial learning rate 0.0128. The learning rate is halved if the loss is not decreasing in 25 epochs. The number of iterations is set to 1000 epochs.

For the Hookean case, the mean squared error (MSE) loss on testing set could be reduced to about $10^{-5} \sim 10^{-8}$ for all the three ODE nets, depending on different random seeds and activation functions used. For the nonlinear pendulum case, the MSE loss on testing set could be reduced to about $10^{-4} \sim 10^{-5}$ for OnsagerNet and $10^{-3} \sim 10^{-5}$ for MLP-ODEN, but only 10^{-2} for SymODEN, see Fig 1. The reason for the low accuracy of SymODEN is that in the SymODEN, the diffusion matrix is assumed to be a function of general coordinate x only [Zhong et al., 2020b], but here in the damped pendulum problem, the diffusion term depends on v . From the test results presented in Figure 1, we see that the results of OnsagerNet are not sensitive to the nonlinear activation functions used. Since the nonlinearities in a lot of dynamical systems are of quadratic or polynomial type, we will only use ReQU and ReQUr as activation functions for other numerical experiments in this paper.

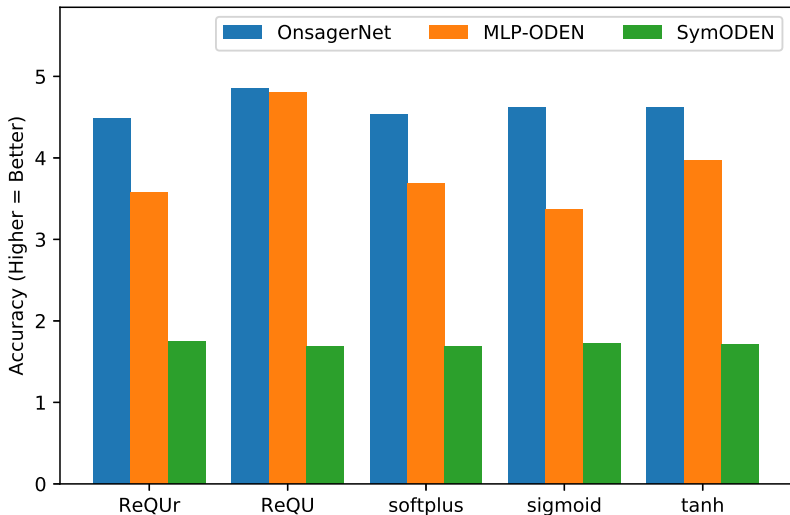
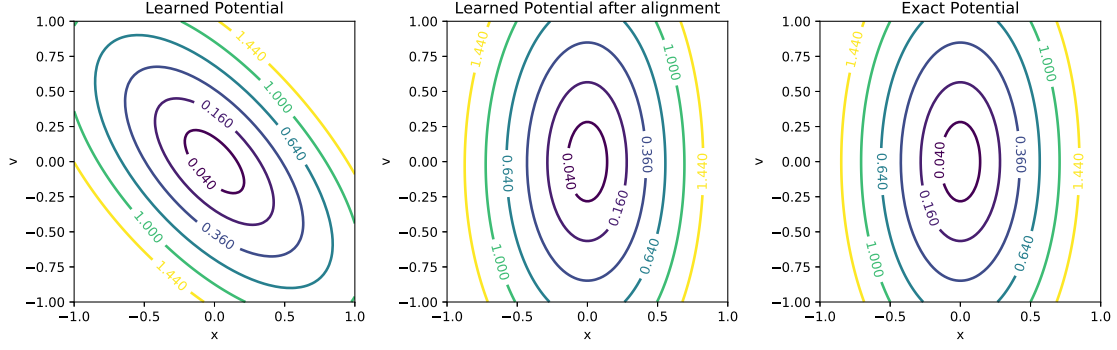


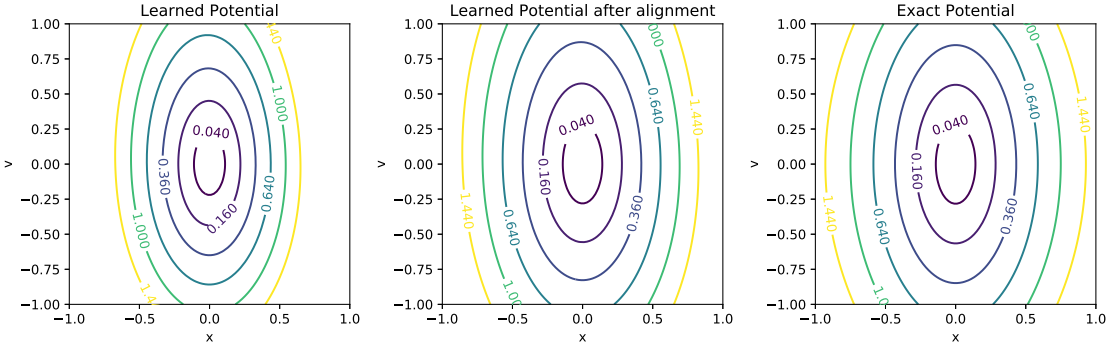
Figure 1: The accuracy of learned dynamics by using three different ODE neural networks and five different activation functions for the nonlinear damped pendulum problem with $\kappa = 4$, $\gamma = 3v^2$. The height of the bars stands for $-\log_{10}$ of the testing MSE. The results are averages of trainings using three different random seeds.

In Fig 2 we plot the contours of learned energy functions using OnsagerNet and compare with the exact ground truth energy function U . We observe a clear correspondence up to rotation and scaling for the linear Hookean model case and a scaling of the nonlinear pendulum case. In all cases, the minimum ($x = 0, v = 0$) is accurately captured. To compare the learned energy with physical energy, we first calculate the Hessian matrix of the energy at origin $(0, 0)$, then make a linear coordinate transformation of the learned energy such that its transformed Hessian at origin is equal to the exact one. After this alignment, the L^2 -norm error between the learned and physical energy for the two tested cases are 2.58×10^{-5} and 6.8×10^{-3} correspondingly.

In Fig. 3, we plot the trajectories for exact dynamics and learned dynamics with initial values start-



(a) Hookean model with $k = 4$, $\gamma = 3$. The L^2 error after alignment is 2.58×10^{-5} .



(b) Pendulum model with $k = 4$, $\gamma = 3|v|^2$. The L^2 error after alignment is 6.8×10^{-3} .

Figure 2: The learned energy functions and the exact energy functions for the Hookean model (a) and the pendulum model (b).

ing from four boundaries of the sample region. We see that the learned dynamics are quantitatively accurate, and the qualitative features of the phase space are also preserved over long times.

4.2 Benchmark problem 2: the Lorenz '63 system

The previous oscillator models have simple Hamiltonian structures, so it is plausible that with some engineering one can obtain a special structured model that works well for such systems. In this section, we consider a target nonlinear dynamical system that may not have such a simple structure. Yet, we will show that owing to the generality of the generalized Onsager principle, OnsagerNet still performs well. Concretely, we consider the well-known Lorenz system [Lorenz, 1963]:

$$\frac{dX}{d\tau} = -\sigma X + \sigma Y, \quad (13)$$

$$\frac{dY}{d\tau} = -XZ + rX - Y, \quad (14)$$

$$\frac{dZ}{d\tau} = XY - bZ, \quad (15)$$

where $b > 0$ is a geometric parameter, σ is the Prandtl number, r is rescaled Rayleigh number.

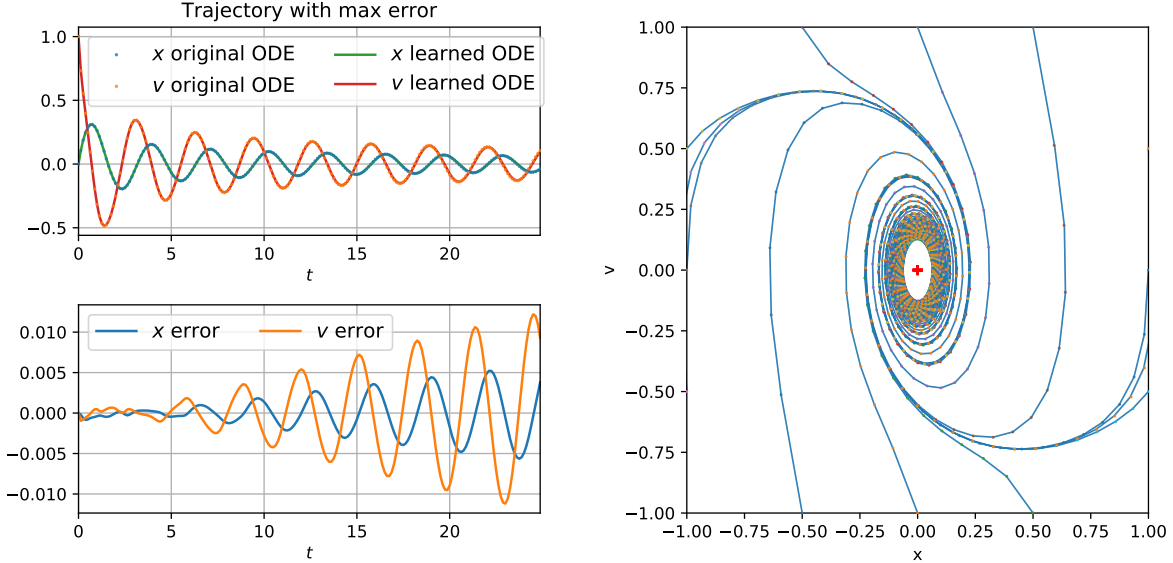


Figure 3: Results of learned ODE model by ReQU OnsagerNet for the nonlinear damped pendulum problem. In the right plot, the dots are trajectory snapshots generated from exact dynamics, the solid curves are trajectories generated from learned dynamics. The red cross is the fixed point numerically calculated for the learned ODE system. Note that the time period of sampled trajectories used to train the OnsagerNet is $T = 5$.

The Lorenz system (13)-(15) is a simple autonomous ODE system that produces chaotic solutions, and its bifurcation diagram is well-studied [Sparrow, 1982, Barrio and Serrano, 2007]. To test the performance of OnsagerNet, we fix $b = 8/3$, $\sigma = 10$, and vary r as commonly studied in the literature. For the $b = 8/3$, $\sigma = 10$ case, the first (pitchfork) bifurcation of the Lorenz system happens at $r = 1$, followed by a homoclinic explosion at $r \approx 13.92$, and then a bifurcation to the Lorenz attractor at $r \approx 24.06$. Soon after, the Lorenz attractor becomes the only attractor at $r \approx 24.74$ (see e.g. [Zhou and E, 2010]). To show that OnsagerNet is able to learn systems with different kinds of attractors and chaotic behavior, we present results for $r = 16$ and $r = 28$.

The procedure of generating sample data and training is similar to the previously discussed case of learning Langevin equations, except that here we set $\alpha = 0.1$, $\beta = 0.1$ and a linear representation for $\hat{f}(h)$ in OnsagerNet. This is because the Lorenz system is a forced system. The result for the case $r = 16$ is presented in Fig 4. We see that both the trajectories and the stable fixed points and unstable limit cycles can be learned accurately. The results for the case $r = 28$ is presented in Fig 5. The largest Lyapunov indices of numerical trajectories (run for sufficient long times) are estimated using a method proposed by Rosenstein et al. [1993]. They are all positive, which suggests that the learned ODE system indeed has chaotic solutions.

Finally, we compare OnsagerNet with MLP-ODEN for learning the Lorenz system. The SymODEN method [Zhong et al., 2020b] cannot be applied since the Lorenz system is non-Hamiltonian. The OnsagerNets used here has one shared hidden layer with 20 hidden nodes, and the total number of trainable parameters is 356. The MLP-ODEN nets have 2 hidden layers with 16 hidden nodes in each layer, with a total 387 tunable parameters. In Fig. 6, we show the accuracy on the test data

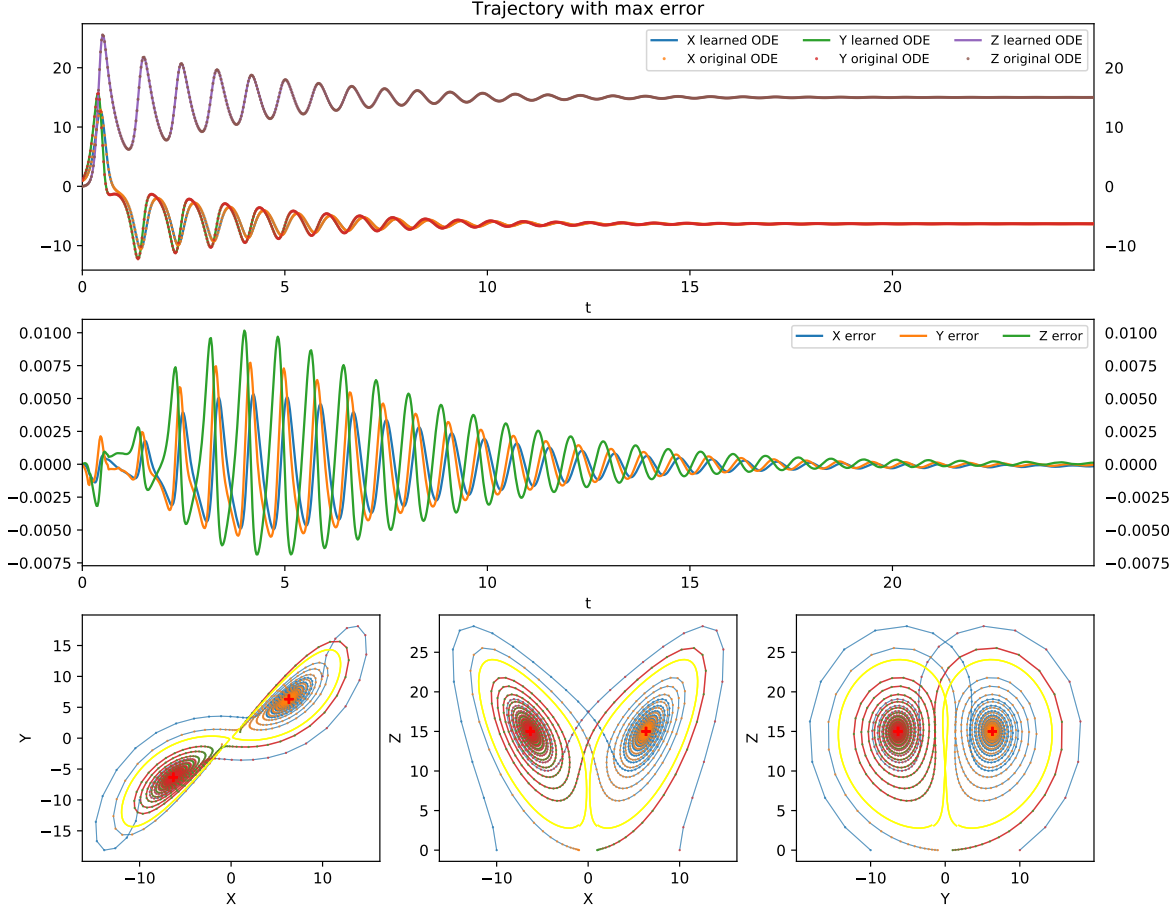


Figure 4: Results of learned ODE model by ReQUR OnsagerNet for the Lorenz system (13)-(15) for $b = 8/3, \sigma = 10, r = 16$. In the bottom three plots, the dots are trajectory snapshots generated from exact dynamics, the solid curves are trajectories generated from learned dynamics, the red one is the one with largest numerical error. The red crosses are the fixed points numerically calculated for the learned ODE system. The yellow closed curves are the unstable limit cycles calculated from the learned ODE system.

set for OnsagerNet and MLP-ODEN using ReQU and ReQUR as activation functions, from which we see OnsagerNet performs much better.

4.3 Application to Rayleigh-Bénard convection

We now discuss the main application of OnsagerNet in this paper, namely learning reduced order models for the 2-dimensional Rayleigh-Bénard convection (RBC) problem, described by the coupled

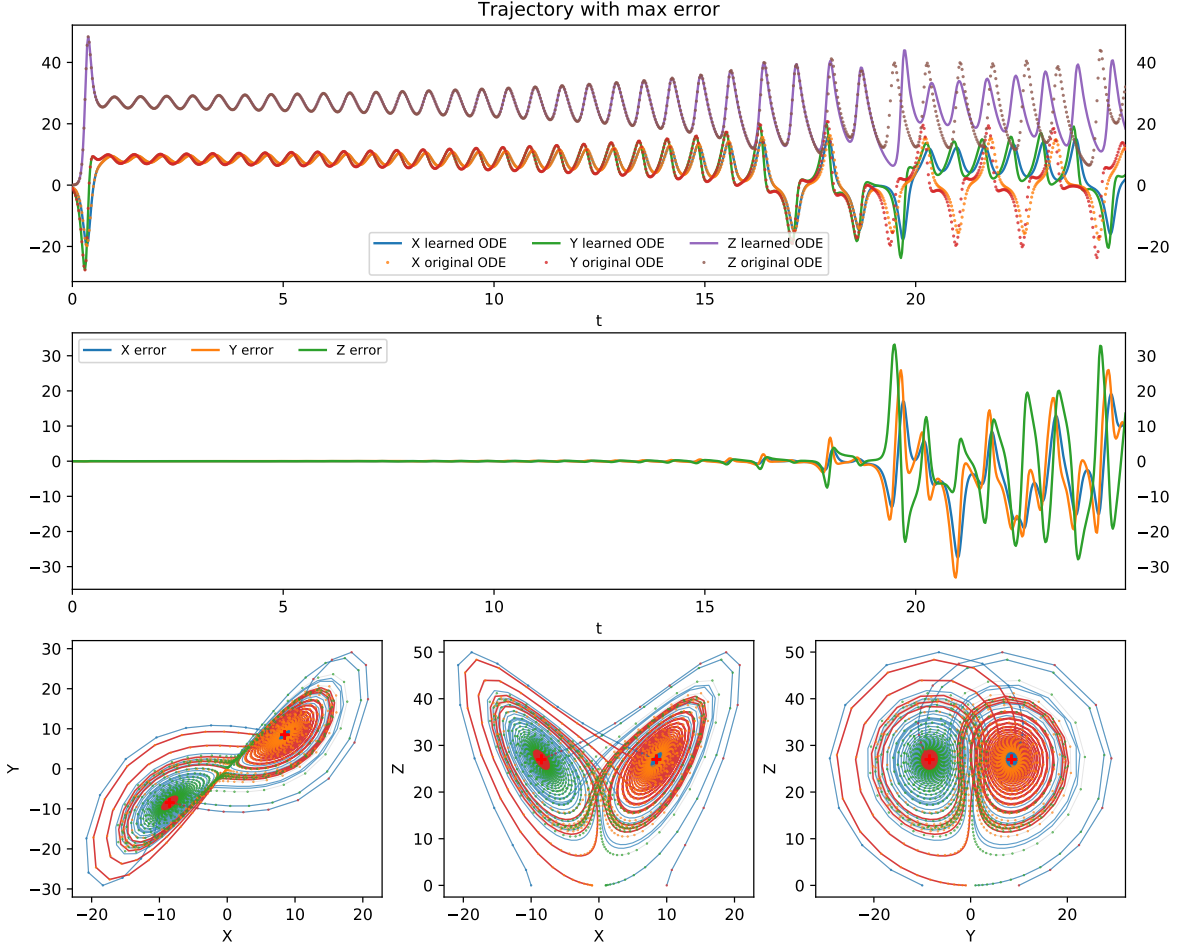


Figure 5: Results of the learned ReQUR OnsagerNet model for the Lorenz system (13)-(15) for $b = 8/3, \sigma = 10, r = 28$. In the bottom three plots, the dots are trajectory snapshots generated from exact dynamics, and the solid curves are trajectories generated from learned dynamics. The red one is the one with largest numerical error. The two red crosses are the (unstable) fixed points numerically calculated for the learned ODE system.

partial differential equations

$$\frac{du}{dt} + (u \cdot \nabla)u = \nu \Delta u - \nabla p + \alpha_0 g \theta, \quad \nabla \cdot u = 0, \quad (16)$$

$$\frac{d\theta}{dt} + u \cdot \nabla \theta = \kappa \Delta \theta + u_y \Gamma, \quad (17)$$

where $u = (u_x, u_y, u_z)$ is the velocity field, $g = (0, g_0, 0)$ the gravitational acceleration, θ the departure of the temperature from the linear temperature profile $\hat{\theta}(y) = \hat{\theta}_H - \Gamma y$, $\Gamma = (\hat{\theta}_H - \hat{\theta}_L)/d$. d is the height of the channel between two plates. The constants g_0, α_0, ν , and κ denote, respectively, the acceleration of gravity, the coefficient of thermal expansion, the kinematic viscosity, and the thermal conductivity. The system is assumed to be homogeneous in z direction, and periodic in x direction, with period L_x .

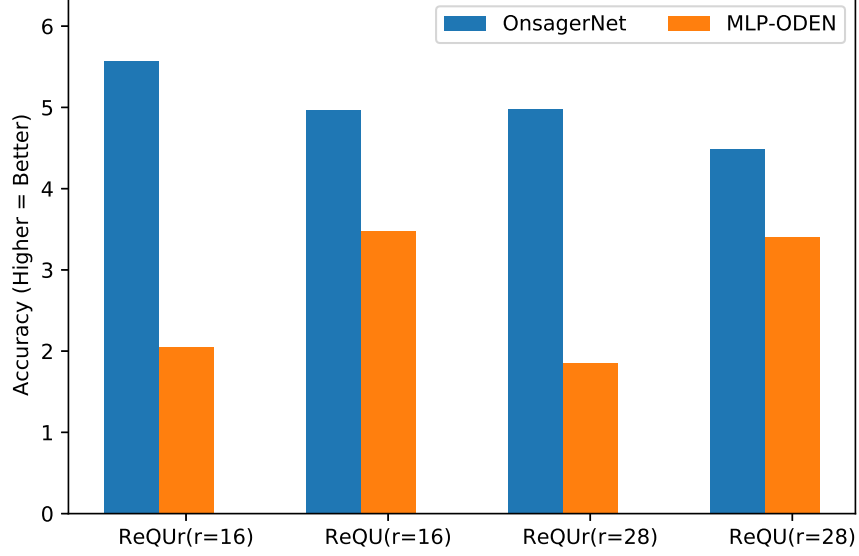


Figure 6: The accuracy of learned dynamics by using OnsagerNets and MLP-ODEN with ReQU and ReQUr as activation functions for learning the Lorenz system with $r = 16, 28$. The height of the bars stands for $-\log_{10}$ of the testing MSE plus 3.5, the higher the better. The results are averages of trainings using three different random seeds.

We will consider the 2D problem by setting $u = (u_x, u_y, 0)$, thus u can be represented by a stream function $\phi(x, y)$:

$$u = (-\partial_y \phi, \partial_x \phi, 0). \quad (18)$$

By eliminating pressure, one gets the following equations for ϕ and θ :

$$\partial_t \Delta \phi - \partial_y \phi \partial_x (\Delta \phi) + \partial_x \phi \partial_y (\Delta \phi) = \nu \Delta^2 \phi + g_0 \alpha_0 \partial_x \theta, \quad (19)$$

$$\partial_t \theta - \partial_y \phi \partial_x \theta + \partial_x \phi \partial_y \theta = \kappa \Delta \theta + \Gamma \partial_x \phi. \quad (20)$$

The solutions ϕ, θ to (19) and (20) have representations in Fourier sine series as

$$\theta(x, y) = \sum_{k_1=-\infty}^{\infty} \sum_{k_2=1}^{\infty} \theta_{k_1 k_2} e^{2i\pi k_1 x / L_x} \sin(\pi k_2 y / d),$$

$$\phi(x, y) = \sum_{k_1=-\infty}^{\infty} \sum_{k_2=1}^{\infty} \phi_{k_1 k_2} e^{2i\pi k_1 x / L_x} \sin(\pi k_2 y / d),$$

where $\theta_{k_1 k_2} = \bar{\theta}_{-k_1 k_2}$ and $\phi_{k_1 k_2} = \bar{\phi}_{-k_1 k_2}$ since θ and ϕ are real. In the Lorenz system, only 3 most important modes ϕ_{11} , θ_{11} and θ_{02} are retained, in this case, the solution have following form

$$\phi(x, y, t) = \frac{(1+a^2)\kappa}{a} \sqrt{2} X(t) \sin(2\pi x / L_x) \sin(\pi y / d), \quad (21)$$

$$\theta(x, y, t) = \frac{R_c \Gamma d}{\pi R} \left(\sqrt{2} Y(t) \cos(2\pi x / L_x) \sin(\pi y / d) - Z(t) \sin(2\pi y / d) \right), \quad (22)$$

where $a = 2d/L_x$, $R = d^4 \frac{g_0 \alpha_0 \Gamma}{\nu \kappa}$ and $R_c = \pi^4(1 + a^2)^3/a^2$. The Lorenz '63 equations (13)-(15) for the evolution of X, Y, Z is obtained by a Galerkin approach [Lorenz, 1963] with time rescaling $\tau = \pi^2 \frac{(1+a^2)}{d^2} \kappa t$, the rescaled Rayleigh number $r = R/R_c$. $b = 4/(1 + a^2)$, and $\sigma = \nu/\kappa$ is the Prandtl number.

Since Lorenz system is aggressively truncated from the original RBC problem, it is not expected to give quantitatively accurate prediction of the dynamics of the original system when r is much larger than 1. Some extensions of Lorenz system to dimensions higher than 3 are proposed, e.g. Curry's 14-dimensional model [Curry, 1978]. But numerical experiments have shown that much large numbers of spectral coefficients need be retained to get quantitatively good results in a Fourier-Galerkin approach [Curry et al., 1984]. In fact, Curry et al. [1984] used more than 100 modes to obtain convergent results for a parameter region similar to $b = 8/3$, $\sigma = 10$, $r = 28$ used by Lorenz. In the following, we show that by using OnsagerNet, we are able to directly learn reduced order models from RBC solution data that are quantitatively accurate and require much less numbers of modes than the Galerkin projection method.

4.3.1 Data generation and equation parameters

We use a Legendre-Fourier spectral method to solve the Rayleigh-Bénard convection problem (16)-(17) based on stream function formulation (19)-(20) to generate sample data. To be consistent with the case considered by Lorenz, we use free boundary condition for velocity. A RBC problem is chosen with the following parameters: $\text{Re} = 10$, $L_x = 4\sqrt{2}$, $\alpha_0 = 0.1$, $g = 9.8$, $\kappa = 0.01$, $\Gamma = 1.17413$. The corresponding Prandtl number, Rayleigh number are $\sigma = 10$, $\text{Ra} = 18410.3$. The relative Rayleigh number is $r = \text{Ra}/R_c = 28$. Initial condition of Lorenz form (21)-(22) is used, where X, Y, Z are sampled from Gaussian distribution and rescaled such that $X^2 + Y^2 + Z^2 \leq R_B$, with R_B a constant.

The semi-discretized Legendre-Fourier system is solved using a second order implicit-explicit scheme with time step-size $\delta t = 0.001$ for 100 time units. 128 real Fourier modes are used for x direction and 49 Legendre modes for y direction. We simulated 100 initial values. The solver outputs 2 snapshots of (u, v, θ) at $(t, t + \delta t)$ for each integer time t .

To have an estimate of the effective dimension, we first apply a PCA to the data. The result is shown in Fig. 11(a). We observe that 99.5% variance are captured by the first 9 principal components, so we expect a good reduced model of dimension less than 10.

4.3.2 The structure of OnsagerNet

The network parameters are similar to that in learning the Lorenz ODE system. Since the Rayleigh-Bénard convection system is not a closed system, we ensure the stability established in Theorem 1 by taking $\alpha = 0.1$, $\beta = 0.1$. To make $\hat{f}(h)$ Lipschitz, we simply let $\hat{f}(h)$ be an affine function of h . We use one common hidden layer (for the $r = 28$ case) which has $n_1 = 2C_{m+2}^m$ hidden nodes for evaluating $L(h), W(h), U_i(h)$ in OnsagerNet, such that polynomials of degree 2 are included in the approximation space if ReQU is used as activation function. We use ReQUr as activation function in this application, it gives slight better training results than ReQU. The ReQUr OnsagerNet is trained by using the standard Adam optimizer [Kingma and Ba, 2015] to minimize the loss with one embedded RK2 step. The embedding of multiple RK2 steps improves the accuracy only a little bit since the time interval of data set $\delta t = 0.001$ is small, the error of RK2 step is not the major

error in the total loss. The use of multiple hidden layers in OnsagerNet also improves accuracy. Since our purpose is to find small models for the dynamics, we only present numerical results of OnsagerNets with one hidden common layer for $r = 28$ case and two hidden common layers for $r = 84$ case, reported next.

4.3.3 Numerical results for $r=28$

We now present numerical results of the RBC problem with $b = 8/3$, $\sigma = 10$, and $r = 28$, a parameter set when used in the Lorenz approximation leads to chaotic solutions, but for the original RBC problems, have only fixed points as attractors. After dimension reduction using PCA for the sample data, we train OnsagerNets using 3, 5, 7, 9 principal components. After the reduced ODE models are learned, we simulate the ODEs using a third order Runge-Kutta method [Shu and Osher, 1988] for one time unit with initial conditions taken from the PCA data at $t_j, j = 0, \dots, 99$, and compare the results to the original PCA data at t_{j+1} . To show the learned ODE system is stable, we also simulate the learned ODE models for 99 time units. We summarize the results in Table 1. More results, including figures of training loss and plots of the errors for individual trajectories are given in Appendix D. From Table 1, we observe that the model using only three variables ($m = 3$) could give good prediction for the period of one time unit, but has a relatively large error for the long time ($t = 99$) prediction. By increasing m gradually to 5, 7, 9, both the short time and long time prediction accuracy increase.

The results of training OnsagerNet together with a stacked auto-encoder and regularized by the isometric loss defined in Eq. (8) are also presented Table 1. The autoencoder we used has 2 hidden encode layers and 2 hidden decode layers with ReQUr as activation functions. From Table 1, we see the results are improved in this ‘‘Autoencoder + OnsagerNet’’ approach, especially for models with less hidden variables and short time prediction results. Notice that the long time prediction results for $m = 9$ is not improved by using the autoencoder. We have tried several other different initializations and random seeds. We randomly got 0 or 1 trajectory failed to converge to the right attractor, i.e. $N_{failed} = 1$ or 0, for $T = 99$ prediction in both ‘‘PCA+ OnsagerNet’’ and ‘‘Autoencoder+OnsagerNet’’ approaches. This can happen when there are some trajectories in the sample data that get very close to some saddle point of the dynamical system. In such a case, even a very small error near a saddle point can produce a very large long time error, and the results become quite unpredictable. This also suggests that for $m \geq 9$, the bottleneck of the learning is the data sampling error, not the model approximation error.

To clearly visualize the numerical errors with respect to time, we show numerical results of simulating a randomly selected trajectory in testing set in Fig. 7. We see that as more and more hidden variables are used, the ODE models learned are more and more accurate, even for long times.

To get an overview of the vector field that drives the learned ODE system, we draw 2-dimensional projections of phase portraits following several representative trajectories in Fig. 8, from which we see there are four stable fixed points, two of which have relatively larger attraction basins, the other two have very small attraction basins. We numerically verified they are all linearly stable by checking the eigenvalues of Jacobian matrices of the learned system at those points. The two fixed points with larger attraction basin are very similar to those appearing in the Lorenz system with $r < 24.06$, which corresponds to the two fixed points resulting from the first pitchfork bifurcation, see, e.g. [Zhou and E, 2010, q_+, q_- in Fig 2.1], and Fig. 4.

Dim Reduction	m	$\text{MSE}_{\text{train}}$	MSE_{test}	$E_{t=1}$	$E_{t=99}$	N_{failed}
PCA	3	3.37(-1)	3.85(-1)	2.58(-2)	2.97(-1)	18
PCA	5	5.12(-2)	7.26(-2)	9.07(-3)	1.17(-1)	7
PCA	7	7.38(-3)	1.36(-2)	2.89(-3)	4.16(-2)	2
PCA	9	5.40(-3)	8.16(-3)	1.87(-3)	4.21(-3)	0
AE+OnsagerNet	3	6.92(-3)	2.94(-2)	5.80(-3)	2.73(-1)	15
AE+OnsagerNet	5	3.03(-3)	1.79(-2)	3.43(-3)	4.68(-2)	3
AE+OnsagerNet	7	1.61(-3)	5.21(-3)	1.69(-3)	1.79(-2)	1
AE+OnsagerNet	9	1.86(-3)	4.42(-3)	1.46(-3)	1.44(-2)	1

Table 1: Numerical results of learning a reduced hidden dynamics for RBC problem. In the first column, “AE+OnsagerNet” stands for results of end-to-end training using an stacked auto-encoder for model reduction and OnsagerNet for reduced dynamics. $\text{MSE}_{\text{train}}$, MSE_{test} represents the MSE loss of the reduced ODE model for training and testing, respectively. $E_{t=1}$, $E_{t=99}$ are the average end-time relative L^2 trajectory errors for solving the learned ODE system from $t = t_j$ to $t = t_j + 1$, and from $t = 0$ to $t = 99$. The N_{failed} in the last column is the number of trajectories (out of 100) in the learned ODE system that do not converge to correct final steady state.

We also test the learned dynamics using OnsagerNet by simulating 100 new numerical trajectories with random initials in the phase space, they all have negative Lyapunov exponents, which suggests that the learned dynamics have no chaotic solutions. This result is consistent to the original RBC system, which also does not exhibit chaos at these parameter values. In this sense, OnsagerNet also preserves the qualitative properties of the full dynamics, despite being embedding in a much lower dimension.

The learned energy function. In Fig. 9, we show the isosurfaces of the learned energy function in the reduced OnsagerNet model for the RBC problem. When PCA data is used, with 3 hidden variables, the energy learned has several local minima, which is very different to a physical energy function one expect for a smooth dynamical system. As the number of hidden variables is increased, the isosurfaces of learned energy function become more and more ellipsoidal, which means the energy is more akin to a positive definite quadratic form, which is consistent to the exact PDE model. This again highlights the preservation of physical principles in the OnsagerNet approach.

4.3.4 A higher Rayleigh number case $r=84$

For $r = 28$, the RBC problem has only fixed points as attractors. To check the robustness of OnsagerNet to approximate dynamics with different properties, we present results of a higher Rayleigh number case with $r = 84$. The corresponding Rayleigh number is 55,230.95. In this case, the RBC problem has four stable limit cycles. However, starting from initial conditions considered by Lorenz’s reduction, the solution needs to evolve for a very long time to get close to the limit cycles. Thus, whether or not the limit sets are limit cycles are not very clear based on only observations of the sample data. An overview of learned dynamics for $m = 11$ is shown in Fig. 10, where four representative trajectories close to the limit cycles together with critical points (saddles)

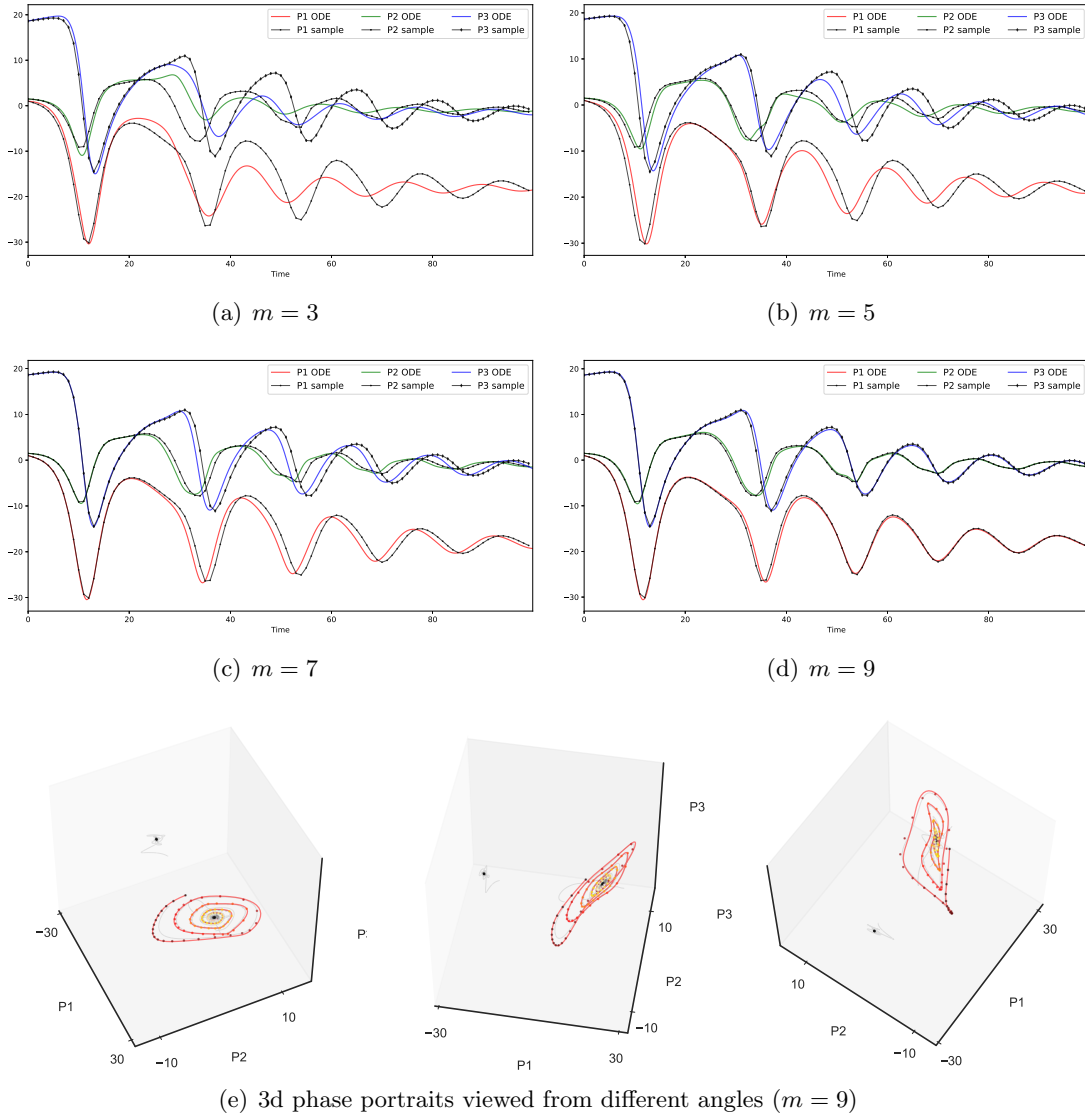


Figure 7: The first 3 principal components of an exact trajectory and the corresponding simulation results of learned reduced models by OnsagerNets with $m = 3, 5, 7, 9$, respectively.

and limit cycles calculated from the learned model are plotted. As before, from this figure we see limit cycles are accurately predicted by reduced order model learned using OnsagerNet. Meanwhile, the saddles could be calculated from the learned OnsagerNet, if they are not far away from the sample data.

More results are given in Appendix D, where ODE solution errors of evolving the sample data for 1 time unit are presented in Fig 15. A typical trajectory in test set and corresponding results by the learned dynamics are plotted in Fig. 16. These results supports the observation that OnsagerNet achieves both quantitative trajectory accuracy and faithfully captures asymptotic behaviors of the original high-dimensional system.

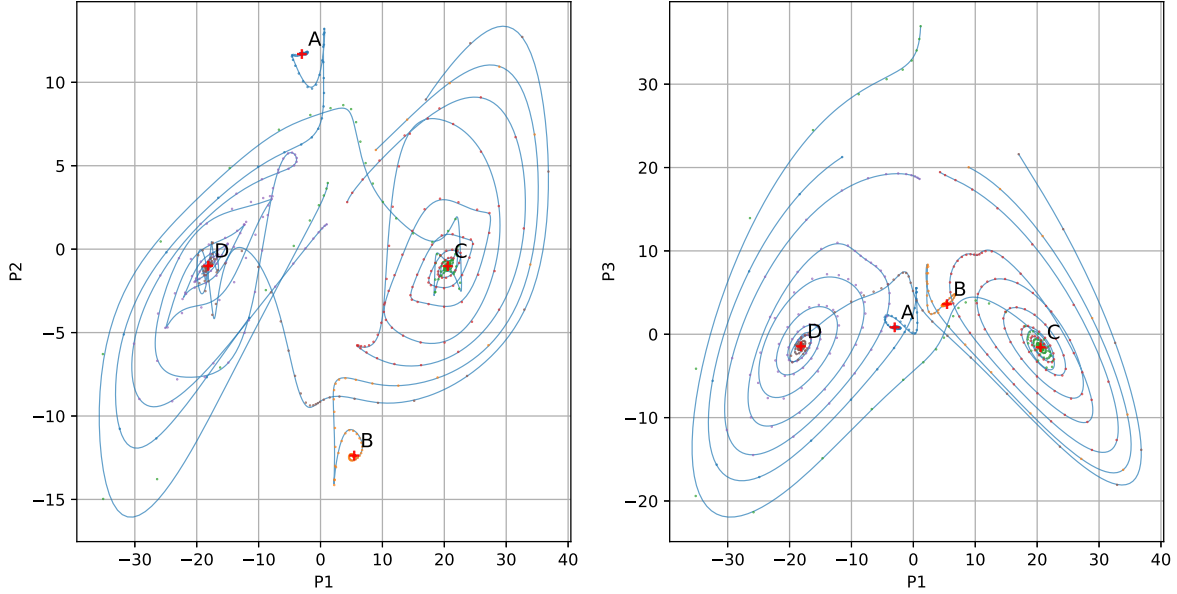
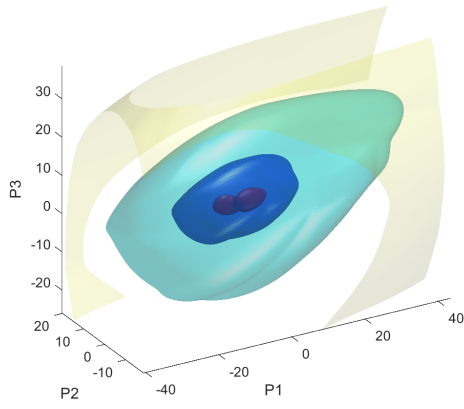


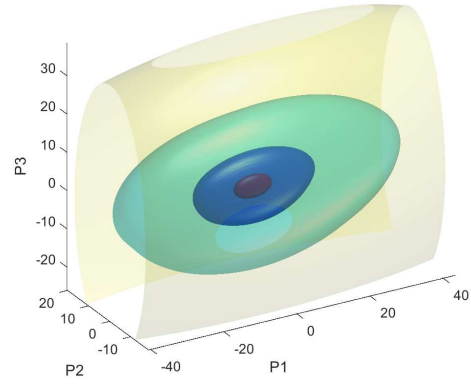
Figure 8: Six representative trajectories from the sample data (colored dots) and the corresponding ODE solutions (solid blue curves) evolved from the same initial values using learned ODE system for the RBC problem with $r = 28$, $m = 9$. The four stable critical points (red crosses) of the learned ODE system are numerically calculated and plotted. Left: projection to (P_1, P_2) plane; Right: projection to (P_1, P_3) plane.

To check whether the learned reduced order model has chaotic solutions, we carried out a numerical estimate of the largest Lyapunov indices of the trajectories in very long time simulations. Here, we did not find any trajectory with a positive Lyapunov index, which suggests that for the parameter setting used, the RBC problem has no chaotic solution, at least for the type of initial conditions considered in this paper.

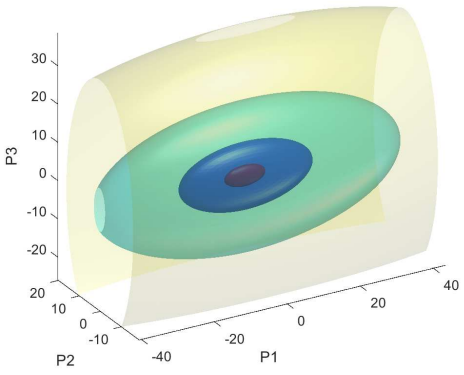
In summary, using the OnsagerNet to learn a reduced model of the RBC equations, we gained two main insights. First, it is possible, under the considered conditions, to obtain an ODE model of relatively low dimension (3-11) that can already capture the qualitative properties (energy functions, attractor sets) while maintaining quantitative reconstruction accuracy. This is in line with Lorenz' intuition in building the model. Second, unlike Lorenz highly truncated model, we show that under the parameter settings investigated, the learned reduced ODE model, while having complex dynamics, does not have chaotic behavior.



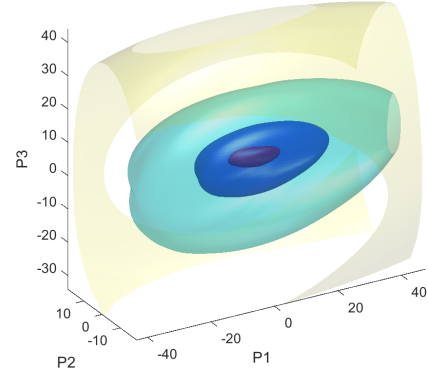
(a) PCA $m = 3$



(b) PCA $m = 5$



(c) PCA $m = 9$



(d) Auto-encoder + OnsagerNet $m = 3$

Figure 9: The learned energy by OnsagerNet with PCA and an autoencoder for RBC problem with $r = 28$. The dependence of the energy function on the first three principal components are shown.

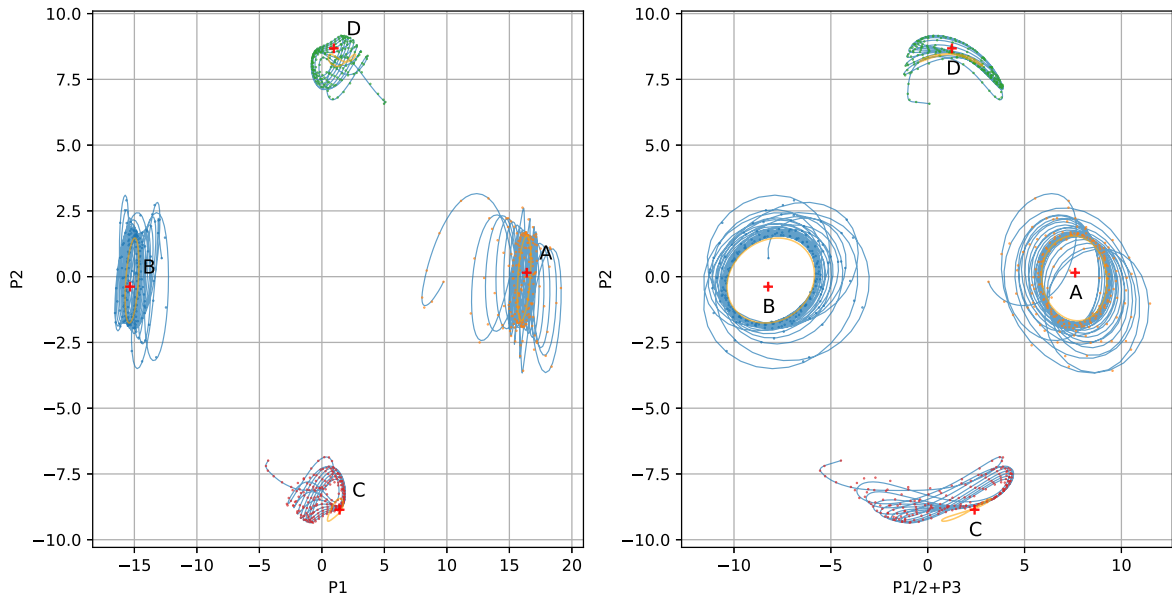


Figure 10: Four representative trajectories from the sample data (colored dots) and the corresponding ODE solutions (solid curves) evolved from the initial values using learned ODE system ($m = 11$) for the case $r = 84$. The four unstable critical points (red crosses) and four stable limit cycles (orange curves) of the learned ODE system are also plotted. Left: projection to (P_1, P_2) plane; Right: projection to $(P_1/2 + P_3, P_2)$ plane.

5 Discussion and summary

We have presented a systematic method to learn stable and interpretable ODE systems or reduced dynamics by a machine learning approach based on a generalized Onsager principle. Comparing to existing methods in the literature, our method has several distinct features.

- Comparing to the non-structured machine learning approaches (e.g. [Bongard and Lipson, 2007, Brunton et al., 2016, Raissi et al., 2018], etc.), the dynamics learned by our approach have precise physical structure, which not only ensures the stability of the learned models automatically, but also gives physically interpretable quantities, such as free energy, diffusive and conservative terms, etc.
- Comparing to the existing structured approach, e.g. the Lyapunov function approach [Kolter and Manek, 2019], symplectic structure approach [Jin et al., 2020, Zhong et al., 2020a], etc., our method, which relies on a principled generalization of the already general Onsager principle, has a more flexible structure incorporating both conservation and dissipation in one equation, which make it suitable for a large class of model reduction problems. In particular, the OnsagerNet structure we impose does not sacrifice short-term trajectory accuracy, but still achieves long term stability and qualitative agreement with the underlying dynamics.
- Different to the linear multi-step method embedded training [Raissi et al., 2018, Xie et al., 2019b] and recurrent neural networks [Pan and Duraisamy, 2018, Wang et al., 2020], we use multiple Runge-Kutta steps embedded in loss function for training. This can handle large and variable data sampling intervals in a straightforward manner.
- We proposed an isometry-regularized autoencoder to find the slow manifold for given trajectory data for dimension reduction, this is different to traditional feature extraction methods such as proper orthogonal decomposition (POD) [Lumley, 1970, Holmes et al., 1996], dynamic mode decomposition (DMD) and Koopman analysis [Schmid [2010], Rowley et al. [2009], Takeishi et al. [2017], which only find important *linear* structures. Our method is also different to the use of an autoencoder with sparse identification of nonlinear dynamics (SINDy) proposed by [Champion et al., 2019] where sparsity of the dynamics to be learned is used to regularize the autoencoder. The isometric regularization allows the autoencoder to be trained separately or jointly with ODE nets. Moreover, it is usually not easy to ensure long-time stability using these type of methods, especially when the dimension of the learned dynamics increases.
- As a model reduction method, different to the closure approximations approach [Wan et al., 2018] that based on Mori-Zwanzig theory [Chorin et al., 2000], which needs to work with an explicit mathematical form of underlying dynamical system and usually leads to non-autonomous differential equations, our approach uses only sampled trajectory data to learn autonomous dynamical systems, the learned dynamics can have very good quantitative accuracy and can be readily be further analyzed with traditional ODE analysis methods, or be used as surrogate models for fast online computation.

We have shown the versatility of OnsagerNet by applying it to identify closed and non-closed ODE dynamics: the nonlinear pendulum and Lorenz system with chaotic attractor, and learn reduced order models with high fidelity for the classical meteorological dynamical systems: the Rayleigh-

Béneard convection problem.

While we did not directly treat noisy data in this paper, this is not expected to be a problem in our approach. This is because, on the one hand for the model reduction problem, the un-resolved part, i.e. the model reduction error, can be regarded as noise. The success of our method in the model reduction problem means it has a certain robustness to noise. On the other hand, for noisy data, we can embed more Runge-Kutta steps at constant step size into the loss function. This increases the effective time of integration, which averages out the noise and increases robustness. Thus, this is an advantage over the linear multi-step approach, which needs to do numerical differentiation that is not robust to noise.

While versatile, the proposed method can be further improved or extended in several ways. For example, in the numerical results of the RBC problem, we see the accuracy is limited by given sample data when we use enough hidden dimensions. One can use an active sampling strategy (see e.g. Zhang et al. [2019], Han et al. [2019]) together with OnsagerNet to further improve the accuracy, especially near saddle points. Furthermore, for problems where transient solutions are of interest but lie on a very high-dimensional space, then directly learning PDEs might be a better approach than learning ODE systems. The learning of PDE using OnsagerNet can be accomplished by incorporating the differential operator filter constraints proposed in [Long et al., 2018] into it, e.g. the diffusive and conservative terms. Finally, for problems where sparsity (e.g. memory efficiency) is more important than accuracy, or a balance between these two are needed, one can either add a l^1 regularization on the weights of OnsagerNets into the training loss function or incorporate sparse identification methods in the OnsagerNet approach.

Acknowledgments

HY would like to thank Prof. Chun Liu, Weiguo Gao, Qi Wang, and Dr. Han Wang for helpful discussions. The work of HY and XT are partially supported by NNSFC Grant 91852116, 11771439. The work of WE is supported in part by a gift from iFlytek to Princeton University. The work of QL is supported by the start-up grant under the NUS PYP programme.

Appendix

A Classical dynamics as generalized Onsager principle

Theorem 2 *Classical Hamilton system with Hamilton given by*

$$H(x, q) = U(x) + \frac{1}{2m}q^2$$

can be written in the form of Eq. (2).

Proof *The Hamilton equation for given H is*

$$\frac{dx}{dt} = \frac{\partial H}{\partial q} = \frac{q}{m},$$

$$\frac{dq}{dt} = -\frac{\partial H}{\partial x} = -\nabla_x U.$$

Taking $M = 0$, $W = \begin{pmatrix} 0 & 1 \\ -1 & 0 \end{pmatrix}$, we have

$$W \begin{pmatrix} \frac{dx}{dt} \\ \frac{dq}{dt} \end{pmatrix} = - \begin{pmatrix} \nabla_x H \\ \nabla_q H \end{pmatrix}.$$

□

Theorem 3 *The deterministic damped Langevin dynamics*

$$m \frac{d^2 x}{dt^2} = -\gamma \frac{dx}{dt} - \nabla_x U(x) \quad (23)$$

can be written in form (2).

Proof Denote $v = \frac{dx}{dt}$, then we have

$$\begin{aligned} \frac{dx}{dt} &= v, \\ m \frac{dv}{dt} + \gamma \frac{dx}{dt} &= -\nabla_x U(x). \end{aligned}$$

By letting $M = \begin{pmatrix} \gamma & 0 \\ 0 & 0 \end{pmatrix}$, $W = \begin{pmatrix} 0 & m \\ -m & 0 \end{pmatrix}$, we have

$$(M + W) \begin{pmatrix} \frac{dx}{dt} \\ \frac{dv}{dt} \end{pmatrix} = - \begin{pmatrix} \nabla_x U(x) \\ mv \end{pmatrix}.$$

This is of form (2) with a new energy (total energy)

$$V(x, v) = U(x) + \frac{m}{2} v^2.$$

□

Theorem 4 *The dynamics described by generalized Poisson brackets, defined below, can be written in form (3). In Poisson bracket approach, the system is described by generalized coordinates (q_1, \dots, q_n) and generalized momentum (p_1, \dots, p_n) . Denote Hamilton of the system as $H(q_1, \dots, q_n; p_1, \dots, p_n)$, then the dynamics of the system is described by the equation [Beris and Edwards, 1994]*

$$F_t = \{F, H\} - [F, H] \quad (24)$$

where F is an arbitrary functional depending on the system variables. The reversible and irreversible contributions to the system are represented by the Poisson bracket $\{\cdot, \cdot\}$ and the dissipation bracket $[\cdot, \cdot]$, respectively, which are defined as

$$\{F, H\} = \sum_{i=1}^n \frac{\partial F}{\partial q_i} \frac{\partial H}{\partial p_i} - \frac{\partial H}{\partial q_i} \frac{\partial F}{\partial p_i},$$

$$[F, H] = J_F M J_F^T, \quad J_F = \left[\frac{\partial H}{\partial q_1}, \dots, \frac{\partial H}{\partial q_n}, \frac{\partial H}{\partial p_1}, \dots, \frac{\partial H}{\partial p_n} \right],$$

where M is symmetric positive semi-definite.

Proof Denote $(h_1, \dots, h_m) = (q_1, \dots, q_n, p_1, \dots, p_n)$, with $m = 2n$. Equation (24) can be written as

$$F_t = (\nabla_h F)^T \frac{dh}{dt} = (\nabla_h F)^T \begin{pmatrix} 0 & I_n \\ -I_n & 0 \end{pmatrix} \nabla_h H - (\nabla_h F)^T M \nabla_h H.$$

By taking $F = (h_1, \dots, h_m)$, such that $\nabla_h F = I_m$, we obtain immediately

$$\frac{dh}{dt} = -W \cdot \nabla_h H - M \cdot \nabla_h H = (M + W)(-\nabla_h H),$$

where $W = \begin{pmatrix} 0 & -I_n \\ I_n & 0 \end{pmatrix}$ is an anti-symmetric matrix, M is a symmetric positive semi-definite matrix, which is of form (3). □

B Generalization of Onsager principle for model reduction

In the original Onsager principle [Onsager, 1931a], [Onsager, 1931b], the system is assumed to be not far away from the equilibrium, such that the system dissipation takes a quadratic form: $\|\frac{dh}{dt}\|_M^2$, i.e. the matrix M is assumed to be constant. In our generalization, we assume M is a general function that depends h . Here we give some arguments why this is necessary and how it can be obtained if some information of the underlying dynamic is given from the viewpoint of model reduction.

To explain nonlinear extension is necessary, we assume that in the underlying dynamics, the matrix M is a constant matrix. The dynamics described by an underlying PDE after spatial semi-discretization takes the form

$$(M + W) \frac{du}{dt} = -\nabla_u V + g, \quad u \in \mathbb{R}^N, \quad (25)$$

where M is a symmetric positive semi-definite *constant* matrix, W is an anti-symmetric matrix. For the dynamics make sense, we need $M + W$ be invertible. $\nabla_u V$ is a column vector of length N . By taking inner product of (25) with $\frac{du}{dt}$, we have an energy dissipation relation of form

$$\frac{dV}{dt} = -\frac{du}{dt} \cdot M \frac{du}{dt} + g \cdot \frac{du}{dt}.$$

Now, suppose that u has a solution in a low-dimensional manifold that could be well described by hidden variables $h(t) \in \mathbb{R}^m$ with $m \ll N$. Denote the low-dimensional solution as $u = u(h(t)) + \varepsilon$, and plug it into (25), we obtain

$$(M + W) \nabla_h u \frac{dh}{dt} = -\nabla_u V(u(h)) + g + O(\varepsilon).$$

Multiplying $(\nabla_h u)^T$ on both sides of the above equation, we have

$$(\nabla_h u)^T (M + W) \nabla_h u \frac{dh}{dt} = -(\nabla_h u)^T \nabla_u V(u(h)) + (\nabla_h u)^T g + O(\varepsilon).$$

So, we obtain an ODE system with model reduction error $O(\varepsilon)$ that is

$$(\hat{M} + \hat{W}) \frac{dh}{dt} = -\nabla_h V + \hat{g}, \quad (26)$$

where

$$\hat{M} = (\nabla_h u)^T M \nabla_h u, \quad \hat{W} = (\nabla_h u)^T W \nabla_h u, \quad \hat{g} = (\nabla_h u)^T g. \quad (27)$$

Note that as long as $\nabla_h u$ has a full column rank, $(\hat{M} + \hat{W})$ is invertible, so the ODE system makes sense. Now \hat{M} , \hat{W} and \hat{g} depend on h in general if $\nabla_h u$ is not a constant matrix. Moreover, if the solutions considered all exist exactly in a low-dimensional manifold, i.e. $\varepsilon = 0$ in the above derivation, then Eq. (26) is exact, which means the generalized Onsager principle is invariant to non-singular coordinate changes.

Remark 1 For underlying dynamics given in the alternative form

$$\frac{du}{dt} = -(M + W) \nabla_u V + f, \quad u \in \mathbb{R}^N. \quad (28)$$

We first rewrite it into form (25) as

$$(M + W)^{-1} \frac{du}{dt} = -\nabla_u V + (M + W)^{-1} f.$$

Then, use same procedure as before to obtain

$$(\nabla_h u)^T (M + W)^{-1} \nabla_h u \frac{dh}{dt} = -(\nabla_h u)^T \nabla_u V(u(h)) + (\nabla_h u)^T (M + W)^{-1} f + O(\varepsilon),$$

from which, we obtains a reduced a model with error $O(\varepsilon)$:

$$\frac{dh}{dt} = -(\hat{M} + \hat{W}) \nabla_h V + \hat{f}, \quad (29)$$

where $\hat{M} = (G + G^T)/2$, $\hat{W} = (G - G^T)/2$, $\hat{f} = G(\nabla_h u)^T (M + W)^{-1} f$, and $G = [(\nabla_h u)^T (M + W)^{-1} \nabla_h u]^{-1}$.

Remark 2 When M, W, g in equation (25) are constant, if linear PCA is used for model reduction, in which $\nabla_h u$ is a constant matrix, then we have $\hat{M}, \hat{W}, \hat{f}$ are constants. However, if we consider the Navier-Stokes equations written in form (25), then M and W are not constant matrices. We obtain nonlinear coefficients in both formulations for the model reduction problem of Navier-Stokes equations.

C Basic properties of non-symmetric positive definite matrices

We present some basic properties of real non-symmetric positive-definite matrices here.

For a $n \times n$ real matrix, we call it *positive definite*, if there exist a constant $\sigma > 0$, such that $x^T A x \geq \sigma x^T x$, for any $x \in \mathbb{R}^n$. If $\sigma = 0$ in the above inequality, we call it *positive semi-definite*.

For any real matrix A , it can be written as a sum of a symmetric part $\frac{A+A^T}{2}$ and a skew-symmetric part $\frac{A-A^T}{2}$. For the skew-symmetric part, we have $x^T \frac{A-A^T}{2} x = 0$, for any $x \in \mathbb{R}^n$. So a non-symmetric matrix is positive (semi-) positive definite if and only if its symmetric part is positive (semi-)definite.

The following theorem is used in deriving OnsagerNet.

Theorem 5 1) Suppose A is a positive semi-definite real matrix, then the real parts of its eigenvalues are all non-negative. 2) The inverse of a non-singular positive semi-definite is also positive semi-definite.

Proof Suppose that $\lambda = \eta + i\mu$ is an eigenvalue of A , the corresponding eigenvector is $z = x + iy$, then

$$Ax + iAy = (\eta x - \mu y) + i(\eta y + \mu x).$$

So

$$\begin{pmatrix} A & 0 \\ 0 & A \end{pmatrix} \begin{pmatrix} x \\ y \end{pmatrix} = \begin{pmatrix} \eta I & 0 \\ 0 & \eta I \end{pmatrix} \begin{pmatrix} x \\ y \end{pmatrix} + \begin{pmatrix} 0 & -\mu I \\ \mu I & 0 \end{pmatrix} \begin{pmatrix} x \\ y \end{pmatrix}.$$

Left multiply the equation by (x^T, y^T) to get (this is the real part of $\bar{z}^T Az = \bar{z}^T \eta z$)

$$x^T Ax + y^T Ay = \eta x^T x + \eta y^T y = \eta(x^T x + y^T y).$$

If A is positive semi-definite, then we obtain $\eta \geq 0$, 1) is proved.

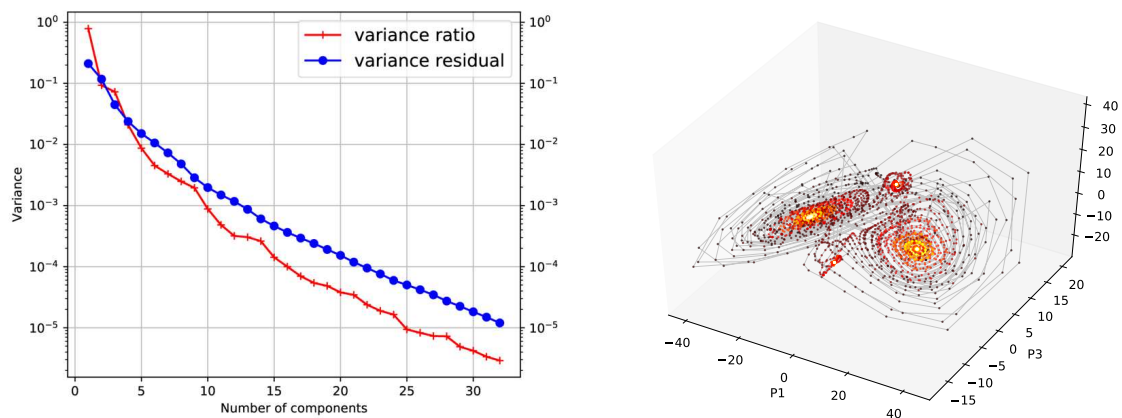
Now suppose that A positive semi-definite and invertible, then for any $x \in \mathbb{R}^n$, we can define y by $Ay = x$ to get

$$x^T A^{-1} x = y^T A^T A^{-1} Ay = y^T A^T y = y^T Ay \geq 0.$$

The second part is proved. □

Note that the inverse of the first part in Theorem 5 is not true. An simple counterexample is $A = \begin{pmatrix} 3 & 2 \\ -2 & -1 \end{pmatrix}$, whose eigenvalues are $\lambda_{1,2} = 1$. But the eigenvalues of its symmetric part are $\lambda_{1,2} = -1, 3$.

D More numerical results and figures



(a) The relative variance of first 32 principal components (PC) (b) The first 3 principal components of the sampled trajectories of Rayleigh-Bénard convection problem.

Figure 11: A peek of the sample data for Rayleigh-Bernard convection problem with $r = 28$, the trajectories are generated using Lorenz type initial values with random amplitude.

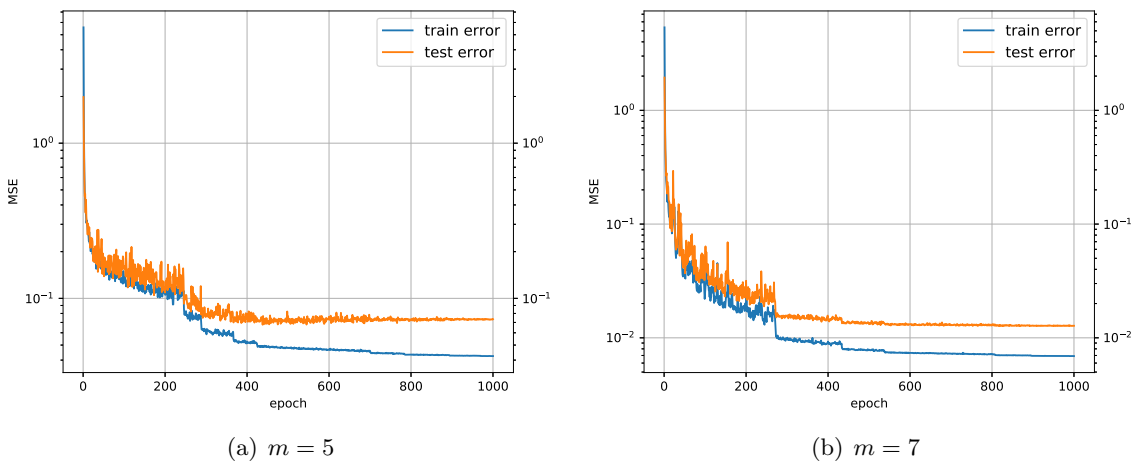


Figure 12: The train loss (blue) and test loss (red) of OnsagerNet to learning hidden dynamics with different m for the RBC problem with $r = 28$.

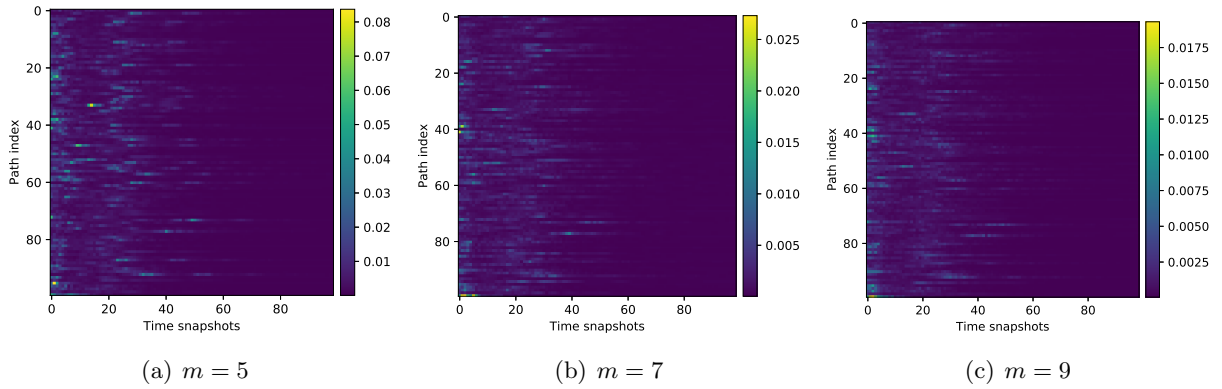


Figure 13: Trajectory prediction errors for 1 time unit using different m for the RBC problem with $r = 28$.

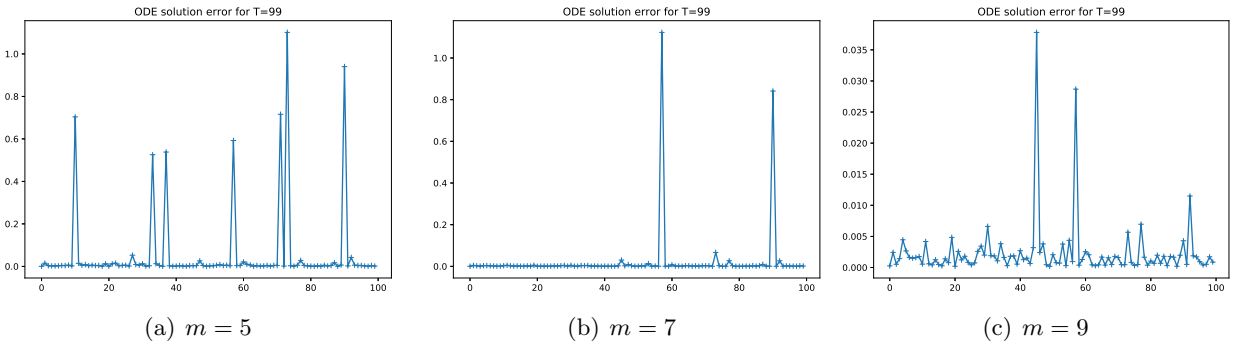


Figure 14: Trajectory prediction errors for 99 time unit using different m for RBC problem with $r = 28$. Note that for $m = 9$ case the maximum error is less than 0.04.

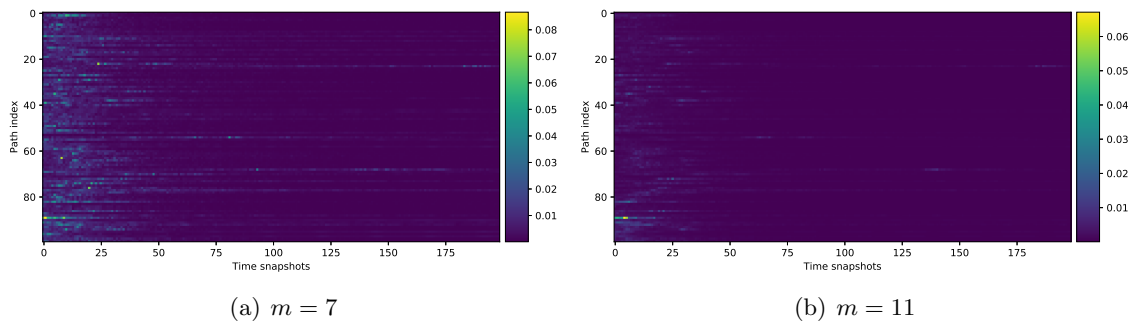


Figure 15: Trajectory prediction errors for 1 time unit using different m for RBC problem with $r = 84$.

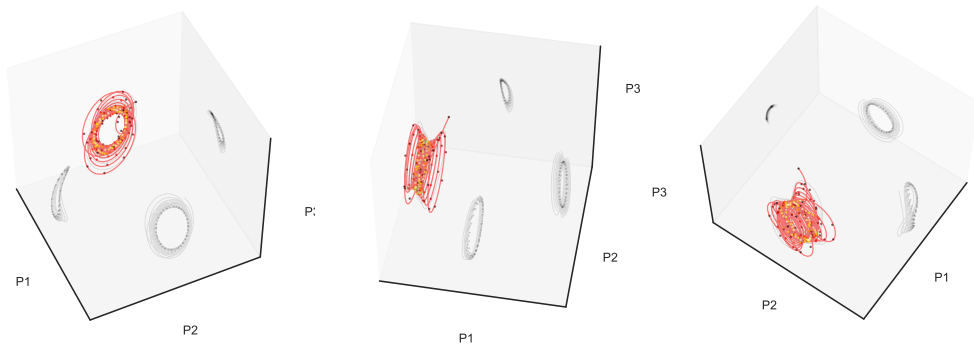
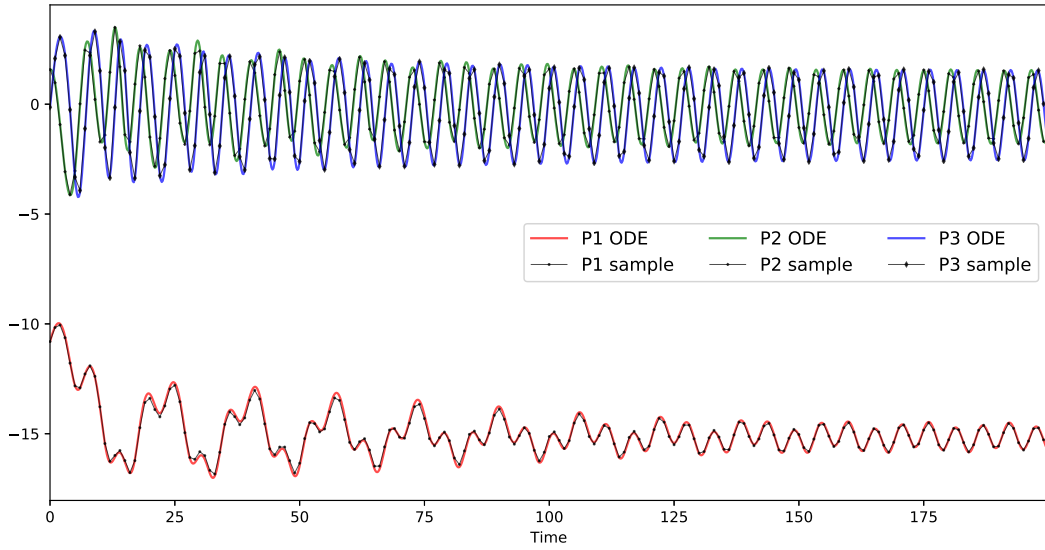


Figure 16: The first 3 principal components of an exact trajectory and the corresponding simulation results of learned reduced models by OnsagerNets trained using 11 principal components for the RBC problem with $r = 84$.

References

- R. Barrio and S. Serrano. A three-parametric study of the Lorenz model. *Physica D*, 229(1):43–51, 2007. doi: 10.1016/j.physd.2007.03.013.
- A. N. Beris and B. Edwards. *Thermodynamics of Flowing Systems*. Oxford Science Publications, New York, 1994.
- J. Bongard and H. Lipson. Automated reverse engineering of nonlinear dynamical systems. *Proc. Natl. Acad. Sci.*, 104(24):9943–9948, 2007. doi: 10.1073/pnas.0609476104.
- S. L. Brunton, J. L. Proctor, and J. N. Kutz. Discovering governing equations from data by sparse identification of nonlinear dynamical systems. *Proc. Natl. Acad. Sci.*, 113(15):3932–3937, 2016. doi: 10.1073/pnas.1517384113.
- K. Champion, B. Lusch, J. N. Kutz, and S. L. Brunton. Data-driven discovery of coordinates and governing equations. *Proc. Natl. Acad. Sci.*, 116(45):22445–22451, 2019. doi: 10.1073/pnas.1906995116.
- A. J. Chorin, O. H. Hald, and R. Kupferman. Optimal prediction and the Mori-Zwanzig representation of irreversible processes. *Proc. Natl. Acad. Sci.*, 97(7):2968–2973, 2000. doi: 10.1073/pnas.97.7.2968.
- J. H. Curry. A generalized Lorenz system. *Commun. Math. Phys.*, 60(3):193–204, 1978. doi: 10.1007/BF01612888.
- J. H. Curry, J. R. Herring, J. Loncaric, and S. A. Orszag. Order and disorder in two- and three-dimensional Bénard convection. *J. Fluid Mech.*, 147:1–38, 1984. doi: 10.1017/S0022112084001968.
- P. G. De Gennes and J. Prost. *The Physics of Liquid Crystals, 2nd Ed., 1993*. Clarendon Press, second edition, 1993.
- S. R. De Groot and P. Mazur. *Non-Equilibrium Thermodynamics*. Dover Publications, 1962.
- M. Doi. Onsager’s variational principle in soft matter. *J. Phys.: Condens. Matter*, 23(28):284118, 2011. doi: 10.1088/0953-8984/23/28/284118.
- M. Doi and S. F. Edwards. *The Theory of Polymer Dynamics*. Oxford University Press, USA, 1986.
- W. E. *Principles of Multiscale Modeling*. Cambridge University Press, New York, 2011.
- D. J. Evans and D. J. Searles. The fluctuation theorem. *Adv. Phys.*, 51(7):1529–1585, 2002.
- M.-H. Giga, A. Kirshtein, and C. Liu. Variational modeling and complex fluids. In Y. Giga and A. Novotny, editors, *Handbook of Mathematical Analysis in Mechanics of Viscous Fluids*, pages 1–41. Springer International Publishing, Cham, 2017.
- M. S. Green. Markoff random processes and the statistical mechanics of time-dependent phenomena. II. Irreversible processes in fluids. *J. Chem. Phys.*, 22(3):398–413, 1954.

- J. Han, Y. Luo, W. Wang, P. Zhang, and Z. Zhang. From microscopic theory to macroscopic theory: A systematic study on modeling for liquid crystals. *Arch. Rational Mech. Anal.*, 215(3): 741–809, 2015. doi: 10.1007/s00205-014-0792-3.
- J. Han, C. Ma, Z. Ma, and W. E. Uniformly accurate machine learning-based hydrodynamic models for kinetic equations. *Proc. Natl. Acad. Sci.*, 116(44):21983–21991, 2019. doi: 10.1073/pnas.1909854116.
- K. He, X. Zhang, S. Ren, and J. Sun. Delving deep into rectifiers: Surpassing human-level performance on ImageNet classification. In *2015 IEEE International Conference on Computer Vision (ICCV)*, pages 1026–1034, Santiago, Chile, 2015. IEEE. doi: 10.1109/ICCV.2015.123.
- G. E. Hinton and R. R. Salakhutdinov. Reducing the dimensionality of data with neural networks. *Science*, 313(5786):504–507, 2006. doi: 10.1126/science.1127647.
- P. Holmes, J. Lumley, and G. Berkooz. *Turbulence, Coherent Structures, Dynamical Systems and Symmetry*. Cambridge Univ Press, 1996.
- W. Jiang, Q. Zhao, T. Qian, D. J. Srolovitz, and W. Bao. Application of Onsager’s variational principle to the dynamics of a solid toroidal island on a substrate. *Acta Mater.*, 163:154–160, 2019. doi: 10.1016/j.actamat.2018.10.004.
- P. Jin, A. Zhu, G. E. Karniadakis, and Y. Tang. Symplectic networks: Intrinsic structure-preserving networks for identifying Hamiltonian systems. *ArXiv200103750*, 2020.
- D. P. Kingma and J. Ba. Adam: A method for stochastic optimization. In *3rd International Conference for Learning Representations, arXiv:1412.6980*, San Diego, 2015.
- J. Z. Kolter and G. Manek. Learning stable deep dynamics models. *33rd Conf. Neural Inf. Process. Syst.*, page 9, 2019.
- M. Kröger and P. Ilg. Derivation of Frank-Ericksen elastic coefficients for polydomain nematics from mean-field molecular theory for anisotropic particles. *J. Chem. Phys.*, 127(3):034903, 2007. doi: 10.1063/1.2743961.
- R. Kubo. Statistical-mechanical theory of irreversible processes. I. General theory and simple applications to magnetic and conduction problems. *J. Phys. Soc. Jpn.*, 12(6):570–586, 1957.
- B. Li, S. Tang, and H. Yu. Better approximations of high dimensional smooth functions by deep neural networks with rectified power units. *Commun. Comput. Phys.*, 27(2):379–411, 2020. doi: 10.4208/cicp.OA-2019-0168.
- Z. Long, Y. Lu, X. Ma, and B. Dong. PDE-Net: Learning PDEs from data. In *35th International Conference on Machine Learning, ICML 2018*, pages 5067–5078, 2018.
- E. N. Lorenz. Deterministic nonperiodic flow. *J. Atmos. Sci.*, 20(2):130–141, 1963.
- J. Lumley. *Stochastic Tools in Turbulence*. Academic Press, 1970.
- C. Ma, J. Wang, and W. E. Model reduction with memory and the machine learning of dynamical systems. *Commun. Comput. Phys.*, 25(4), 2019. doi: 10.4208/cicp.OA-2018-0269.
- L. Onsager. Reciprocal relations in irreversible processes. I. *Phys. Rev.*, 37:405, 1931a.

- L. Onsager. Reciprocal relations in irreversible processes. II. *Phys. Rev.*, 38:2265, 1931b.
- H. C. Ottinger. *Beyond Equilibrium Thermodynamics*. John Wiley & Sons, 2005.
- S. Pan and K. Duraisamy. Data-driven discovery of closure models. *SIAM J. Appl. Dyn. Syst.*, 17(4):2381–2413, 2018. doi: 10.1137/18M1177263.
- A. Paszke, S. Gross, F. Massa, A. Lerer, J. Bradbury, G. Chanan, T. Killeen, Z. Lin, N. Gimeshein, L. Antiga, A. Desmaison, A. Kopf, E. Yang, Z. DeVito, M. Raison, A. Tejani, S. Chilamkurthy, B. Steiner, L. Fang, J. Bai, and S. Chintala. PyTorch: An imperative style, high-performance deep learning library. In *Advances in Neural Information Processing Systems 32*, pages 8026–8037. Curran Associates, Inc., 2019.
- T. Qian, X.-P. Wang, and P. Sheng. A variational approach to moving contact line hydrodynamics. *J. Fluid Mech.*, 564:333–360, 2006.
- M. Raissi, P. Perdikaris, and G. E. Karniadakis. Multistep neural networks for data-driven discovery of nonlinear dynamical systems. *ArXiv180101236*, 2018.
- L. Rayleigh. On the instability of jets. *P. Lond. Math. Soc.*, s1-10(1):4–13, 1878. ISSN 1460-244X. doi: 10.1112/plms/s1-10.1.4.
- S. J. Reddi, S. Kale, and S. Kumar. On the convergence of Adam and beyond. In *International Conference on Learning Representations*, 2018.
- S. Rifai, P. Vincent, X. Muller, X. Glorot, and Y. Bengio. Contractive auto-encoders: Explicit invariance during feature extraction. *Proceedings of the 28th International Conference on Machine Learning*, page 8, 2011.
- M. T. Rosenstein, J. J. Collins, and C. J. De Luca. A practical method for calculating largest Lyapunov exponents from small data sets. *Physica D*, 65(1-2):117–134, 1993. doi: 10.1016/0167-2789(93)90009-P.
- C. W. Rowley, I. Mezić, S. Bagheri, P. Schlatter, and D. S. Henningson. Spectral analysis of nonlinear flows. *J. Fluid Mech.*, 641:115–127, 2009. doi: 10.1017/S0022112009992059.
- P. J. Schmid. Dynamic mode decomposition of numerical and experimental data. *J. Fluid Mech.*, 656:5–28, 2010. doi: 10.1017/S0022112010001217.
- M. Schmidt and H. Lipson. Distilling free-form natural laws from experimental data. *Science*, 324(5923):81–85, 2009. doi: 10.1126/science.1165893.
- C.-W. Shu and S. Osher. Efficient implementation of essentially non-oscillatory shock-capturing schemes. *J. Comput. Phys.*, 77(2):439–471, 1988. doi: 10.1016/0021-9991(88)90177-5.
- C. Sparrow. *The Lorenz Equations: Bifurcations, Chaos, and Strange Attractors*. Springer-Verlag, New York, 1982. doi: 10.1007/978-1-4612-5767-7.
- N. Takeishi, Y. Kawahara, and T. Yairi. Learning Koopman invariant subspaces for dynamic mode decomposition. In *Advances in Neural Information Processing Systems 30*, pages 1130–1140. Curran Associates, Inc., 2017.

- Z. Y. Wan, P. R. Vlachas, P. Koumoutsakos, and T. P. Sapsis. Data-assisted reduced-order modeling of extreme events in complex dynamical systems. *PLoS ONE*, 13(5):e0197704, 2018. doi: 10.1371/journal.pone.0197704.
- Q. Wang, N. Ripamonti, and J. S. Hesthaven. Recurrent neural network closure of parametric POD-Galerkin reduced-order models based on the Mori-Zwanzig formalism. *J. Comput. Phys.*, 410:109402, 2020. doi: 10.1016/j.jcp.2020.109402.
- C. Xie, K. Li, C. Ma, and J. Wang. Modeling subgrid-scale force and divergence of heat flux of compressible isotropic turbulence by artificial neural network. *Phys. Rev. Fluids*, 4(10), 2019a. doi: 10.1103/PhysRevFluids.4.104605.
- X. Xie, G. Zhang, and C. G. Webster. Non-intrusive inference reduced order model for fluids using linear multistep neural network. *Mathematics*, 7(8), 2019b. doi: 10.3390/math7080757.
- X. Yang, J. Li, M. Forest, and Q. Wang. Hydrodynamic theories for flows of active liquid crystals and the generalized Onsager principle. *Entropy*, 18(6):202, 2016. doi: 10.3390/e18060202.
- H. Yu, G. Ji, and P. Zhang. A nonhomogeneous kinetic model of liquid crystal polymers and its thermodynamic closure approximation. *Commun. Comput. Phys.*, 7(2):383, 2010. doi: 10.4208/cicp.2009.09.202.
- L. Zhang, D. Y. Lin, H. Wang, R. Car, and W. E. Active learning of uniformly accurate interatomic potentials for materials simulation. *Physical Review Materials*, 3(2):023804, 2019.
- J. Zhao, X. Yang, Y. Gong, X. Zhao, X. Yang, J. Li, and Q. Wang. A general strategy for numerical approximations of non-equilibrium models—part I: Thermodynamical systems. *Int. J. Numer. Anal. Model.*, 15(6):884–918, 2018.
- Y. D. Zhong, B. Dey, and A. Chakraborty. Dissipative SymODEN: Encoding Hamiltonian dynamics with dissipation and control into deep learning. *arXiv:2002.08860*, 2020a.
- Y. D. Zhong, B. Dey, and A. Chakraborty. Symplectic ODE-Net: Learning Hamiltonian dynamics with control. *ICLR 2020, ArXiv190912077*, 2020b.
- X. Zhou and W. E. Study of noise-induced transitions in the Lorenz system using the minimum action method. *Commun. Math. Sci.*, 8(2):341–355, 2010.